ABSTRACT

INFLUENCE OF SURFACTANT ON THE BREAKUP OF A FLUID JET IN VISCOUS SURROUNDING

by
Muhammad Irfan Hameed

The effect of insoluble surfactant on the breakup of a fluid jet surrounded by another viscous fluid at low Reynolds number is studied both theoretically and experimentally. Equations governing the evolution of the interface and surfactant concentration are derived using a long wavelength approximation for the case of an inviscid jet and a slightly viscous jet surrounded by a more viscous fluid. These one dimensional partial differential equations governing the evolution of the slender jet are solved numerically for given initial interfacial perturbations and surfactant concentration. It is found that the presence of insoluble surfactant at the interface retards the pinch-off. The influence of surface diffusion of surfactant on the jet deformation is studied by varying surface Peclet number. It is found that greater diffusion of surfactant causes the jet to pinch faster. To check the predictions of our model, we performed experiments both for clean interface and as well as in presence of surfactants. The experimental results support the prediction of the theoretical model that the presence of surfactant slows down the pinch-off process. Results of the long wavelength model are also compared against the numerical simulations of the full problem. The solution of the full problem shows similar behavior to the simplified long wavelength model.

INFLUENCE OF SURFACTANT ON THE BREAKUP OF A FLUID JET IN VISCOUS SURROUNDING

by
Muhammad Irfan Hameed

A Dissertation
Submitted to the Faculty of
New Jersey Institute of Technology and
Rutgers, The State University of New Jersey – Newark
in Partial Fulfillment of the Requirements for the Degree of
Doctor of Philosophy in Mathematical Sciences

Department of Mathematical Sciences, NJIT
Department of Mathematics and Computer Science, Rutgers-Newark

May 2005

APPROVAL PAGE

INFLUENCE OF SURFACTANT ON THE BREAKUP OF A FLUID JET IN VISCOUS SURROUNDING

Muhammad Irfan Hameed

Prof. Michael Siegel, Dissertation Advisor
Associate Professor of Mathematics, NJIT — Date

Prof. Demetrios Papageorgiou, Committee Member
Professor of Mathematics, NJIT — Date

Prof. Robert Miura, Committee Member
Professor of Mathematics, NJIT — Date

Prof. Michael Booty, Committee Member
Associate Professor of Mathematics, NJIT — Date

Prof. Charles Maldarelli, Committee Member
Professor of Chemical Engineering, CUNY — Date

BIOGRAPHICAL SKETCH

Author: Muhammad Irfan Hameed

Degree: Doctor of Philosophy

Date: May 2005

Undergraduate and Graduate Education:

- Doctor of Philosophy in Mathematical Sciences,
  New Jersey Institute of Technology, Newark, NJ, 2005
- Master of Science in Applied Mathematics,
  New Jersey Institute of Technology, Newark, NJ, 2004
- Master of Philosophy,
  Quaid-i-Azam University, 2000

Major: Mathematical Sciences

Presentations and Publications:

To My Loving Parents

ACKNOWLEDGMENT

It is my pleasure and honor to express my sincerest gratitude to my learned advisor Professor Michael Siegel under whose dynamic supervision, propitious guidance and illustrative advice, the research work present in this dissertation became possible. His deep knowledge and logical way of thinking have been of a great value for me. He showed me different ways to approach a research problem and the need to be persistent to accomplish any goal. Without his generous encouragement and patient guidance, I would not have been able to complete this work. In short, he proved to be a perfect model of professionalism, understanding and having a wealth of knowledge and commitment to the subject.

My profound thanks, gratitude and reverence is due to Professor Dimitrios Papageorgiou for his keen interest, inspiring guidance, and consistent encouragement. This work without his expert advice and help would be incomplete. I am lucky that I had an opportunity to have him as my teacher, advisor and well wisher.

Special thanks are due to Professor Charles Maldarelli, Benjamin Levich Institute, New York for introducing me to the amazing world of experimental fluid dynamics. His innovative ideas, valuable suggestions and fruitful discussions helped me lot to improve the quality of the present research work.

I would also like to thank Professor Robert Miura and Professor Michael Booty for agreeing to be on my committee, for carefully reading the thesis and for their suggestions and corrections.

I would like to thank Professor Daljit Singh Ahluwalia, for providing support, guidance and advice throughout my stay at NJIT. I am grateful to Department of Mathematical Sciences, NJIT, for providing me financial support during my studies.

The nice company of my class-fellows and friends always proved to be a source of inspiration and encouragement. I would like to say thanks to all my class-fellows

for their support and encouragement during my stay here. I especially want to thank my time tested friends Jyoti Champanirkar, Lin Zhou, Christina Ambrosio, Arnaud Goullet, Dmitri Tseluiko and Xing Li Wang.

I would like to thank the ever smiling administrative staff of the Department of Mathematical Sciences at NJIT, Ms. Padma Gulati, Ms. Susan Sutton, Ms. Liliana Boland and Ms. Sherri Brown, for their warm support and for making the life easier for graduate students. I would especially like express my thanks and gratitude to Ms. Gulati for her immense help and moral support throughout these years. She was always there to get me out of troubles and help me solve my problems.

This study would have been impossible without the prayers, love and affection of my family. I wish to express my appreciation and deep sense of gratitude from the core of my heart to my sweet parents, loving brothers and sisters and my congenial friend Nadeem, who's hands always arise in prayers for my success.

TABLE OF CONTENTS

TABLE OF CONTENTS
(Continued)

Chapter **Page**

LIST OF FIGURES

LIST OF FIGURES
(Continued)

Figure **Page**

CHAPTER 1

INTRODUCTION

The breakup of a fluid jet or a bubble surrounded by another viscous fluid has been of great interest to physicists and engineers due to industrial and biomedical applications. For example, the surface tension driven breakup of liquid-liquid and liquid-gas jets are common in many industrial applications, including ink-jet printers, chemical reactors and solderjet technology [2]. Bubble deformation and breakup is important in the processing of polymer melts and emulsion formation [30].

The problem of jet breakup has been extensively studied both experimentally and theoretically for jets injected into air, where the air is modeled as a vacuum or inviscid fluid. These types of fluid jets are called single fluid jets. For the case of single fluid jets, the theoretical development started with the classical work of Rayleigh [28] who studied the breakup of an infinite free inviscid jet injected into air. Rayleigh analyzed the breakup of the liquid jet using linear stability theory and calculated the growth of infinitesimal periodic disturbances on a stationary liquid cylinder. Weber [37] extended the linear theory to the case of viscous jets. In both of the above cases, it was shown that a cylindrical fluid column is unstable under axisymmetric perturbations whose wavelength is greater than the circumference of the undisturbed jet.

Although the linear theory describes well the early stages of jet evolution, it does not properly account for the breaking process and drop formation, which are non-linear phenomena. After the initial work of Rayleigh and Weber, subsequent experimental and theoretical investigations have focused on elucidating details of the breakup of a single fluid jet. Recently, Eggers [10] used a long wavelength approximation of the incompressible Navier-Stokes equations to study the viscous jet

pinch-off in an inviscid environment. He showed that the dynamics of the pinching thread is governed by a balance between the axial gradient of the capillary pressure $\frac{\sigma}{R}$, axial acceleration, and viscous stresses. Eggers found similarity solutions to the long wave equations that describe the jet pinch-off, in which axial length scale shrinks according to $\frac{z}{L} \sim (\frac{\tau}{T})^{\frac{1}{2}}$, while the jet radius decreases as $\frac{R}{L} \sim \frac{\tau}{T}$, where τ is the time to pinch-off, T and L are suitably defined time and length scales. Note that the ratio of the radial to axial lengths scales is small, consistent with the long wave approximations.

Papageorgiou [25] analyzed the one dimensional long wave equations derived from the Stokes equations, i.e., neglecting inertia. Near the pinch-off, scalings were found which correspond to a viscous-capillary balance, and are different from the scalings in the inertial case. Similarity solutions based on these scalings show that the jet pinches-off with a smooth profile in finite time. A recent review paper by Eggers [11] presents a comprehensive review of non-linear theories and experimental studies on the surface tension driven single fluid jet, including pinch-off.

For the case of two fluid jets, the effects of the surrounding fluid must be included in the analysis of the jet instability and breakup. In this case, additional non-trivial effects enter due to the presence of the outside continuous phase. The first work in the case of two fluid jets is due to Tomotika [36], who derived a relationship between the growth rate and the wave number of the disturbance. Tomotika found that the criterion for instability of Rayleigh [28] and Weber [37], originally derived for the single fluid jet, does not change when the outer fluid is present. Lister and Stone [19] considered the effect of a viscous external fluid on the non-linear dynamics and breakup of a fluid jet evolving under Stokes flow. They found that when the external fluid viscosity is introduced, the dynamics near the pinch-off is given by a balance between capillary pressure, interior and exterior viscous stresses. In this case, the jet pinches according to the scalings $z \sim \lambda^{\frac{1}{2}}(\frac{\sigma}{\mu_i})\tau$ and $h \sim \frac{\sigma}{\mu_i}\tau$, where σ is the

surface tension, μ_i is the inside viscosity and $\lambda = \frac{\mu_i}{\mu_o}$ is the viscosity ratio. For these scalings to hold it is required that $\lambda \geq 1$. Lister and Stone [19] employed a boundary integral numerical method to verify these scalings when the viscosity ratio $\lambda = 1$. It is important to note that these scalings show that the two fluid dynamics does not satisfy the long wave assumption since $h \sim \frac{z}{\lambda^{\frac{1}{2}}}$, for $\lambda \geq 1$. Zhang [41], [42] extended the numerical results of Lister and Stone to $\frac{1}{16} \leqslant \lambda \leqslant 16$, while Lister and Sierou [32] introduced similarity variables into the boundary integral simulations to determine the self similar shapes for smaller values of λ. Experiments of Cohen et al. [5] are comparable with the numerical results of Zhang. Most recently, Doshi et al. [8] used experiments, large scale numerical simulations and asymptotic analysis to study the breakup of a low viscosity jet inside a highly viscous exterior fluid and showed that different initial and boundary conditions lead to different asymptotic profiles when the interior viscosity is small enough. Howell and Siegel [15] generalized the above results to consider the cases in which the jet is not axisymmetric and is driven by a transverse straining flow.

The presence of surfactant in surface tension driven flows is important from the industrial point of view yet less is known about the fine details of the jet breakup under the influence of surfactants. Surfactants are surface active agents which are present in nearly all liquids in the form of impurities and contaminations. Their presence at the interface can significantly alter the interfacial properties. In some cases, they are added to control the fluid behavior while in other situations their presence may not be desirable but they are difficult to remove from the system. It is important therefore, to understand the effect of surfactants on the dynamics of jet breakup.

There have been few studies to understand the influence of surfactants on the breakup of two fluid jets. Whitaker [39] first investigated the effect of a surfactant on a fluid filament surrounded by a gas using linear stability theory. Stone et

al. [34] and Milliken [22] considered the effect of a surfactant on the deformation and breakup of a drop in extensional flow and established a qualitative relationship between the flow, surfactant concentration and surface stresses. Kwak and Pozrikidis [18] investigated the effect of surfactants on the stability of a liquid thread. They carried out the linear stability analysis for axisymmetric perturbations in the absence or presence of fluid inertia. They also studied the non-linear instability of the infinite thread under the conditions of Stokes flow, using numerical simulations employing boundary integral method. They found that the presence of surfactant substantially decreases the growth rate of instability. Later, Kwak et al. [17] extended the above analysis to consider the case of an extensional flow. Hansen et al. [14] presented a thorough analysis of the linear stability of a fluid filament embedded in a viscous fluid in the presence of a soluble surfactant. Later on, Lister et al. [35] also used linear stability analysis as well as one-dimensional non-linear approximations to the Navier-Stokes equations to study the surface tension driven flow of a liquid jet in inviscid surrounding. Lister et al. concluded that for a fluid jet in inviscid surroundings, surfactants have little effect on the pinch-off since the flow in the jet sweeps the surfactant away from the pinch point due to advection. However, this is not necessarily the case when there is no internal fluid, or the internal fluid is much less viscous than the outer fluid. Craster et al. [7] studied the effect of surfactant on the pinch-off and satellite formation of a viscous thread. They found that the size of satellite formed during the thread breakup decreases with the increase of initial surfactant concentration. The previously observed self-similar pinch-off for the case of no surfactant [10] was preserved in the presence of surfactant.

The role of surface active agents in liquid-liquid and liquid-gas systems has attracted the attention of many experimentalists over the years. Pan et al. [24] performed the experiments to measure the kinetic rate constants for the surfactant exchange at air/water interface. Fang and Shah [12] studied the effect of surfactant

on the heat transfer through air/water and water/oil interfaces using image analysis technique to show that the surfactant monolayer introduces a noticeable heat transfer resistance to the heat transfer forces across the interface. Jet pinch-off and drop formation in liquid-liquid system has also been studied by Webster and Longmire [38]. They investigated the behavior of a glycerol/water jet flowing into Dow Corning fluid under the action of superposed sinusoidal perturbation. The forcing frequency is found to have a dramatic effect on the size, spacing and number of drops resulting from the jet breakup. In a recent experimental investigation, Rothert et al. [29] observed the drop pinch-off at a nozzle for different viscosities and investigated three consecutive flow regimes. They found that close the pinch point the profiles become self-similar at a certain time.

To gain insights into two-fluid pinch-off with variable surface tension, we study the effect of insoluble surfactant on the breakup of an inviscid and a slightly viscous jet in highly viscous exterior fluid. To approximate the solution of the full Stokes equations, we use a very different approach based upon the slender body theory, which exploits the large aspect ratio of the jet using slenderness ratio ϵ as an expansion parameter. Due to the linearity of the Stokes equations, an exact solution can be written as an integral of a distribution of point forces, or Stokeslets over the boundary of a fluid region. This is true for the case of both moving and stationary boundaries. When the geometry of the fluid is characterized by a small aspect ratio, an approximation to the flow outside is given by replacing the point forces on its boundary by a distribution of point forces and other singularities along the centerline of the body. If the slender inhomogeneity is deformable, as in our case, the singularities required are the point mass sources and point forces alone. The flow induced by these singularities is given by the superposition of the corresponding fundamental solutions or the free space Green's functions.

Slender body theory has been successfully employed to study Stokes flow in different geometries. Buckmaster [4] used slender body theory to study the deformation of an inviscid drop in an axisymmetric straining flow and found that there were many possible steady shapes of the droplet. Acrivos and Lo [1] refined the studies of Buckmaster and showed that all but one of those steady shapes are unstable. Keller and Rubinow [16] have developed a non-local slender body approximations that captures the global effect on the fluid velocity arising from the presence of a thin filament. This approach introduces an integral equation with a modified Stokeslet kernel on the filament centerline that relates the filament forces to the velocity of the centerline.

With an aim to better understand the pinch-off dynamics under the influence of variable surface tension, we use slender body theory, numerical simulations and experimental studies to investigate the effect of surfactant on the necking and breakup. In the first part, we consider a slender axisymmetric fluid jet of inviscid fluid surrounded by a viscous outer fluid in the presence of insoluble surfactant at the interface. The inner phase is an inviscid gas, and the outer phase is a viscous fluid. The effect of the interior inviscid fluid on the exterior viscous fluid is accounted for by the spatially uniform pressure $p(t)$. Dynamics exterior to the jet are governed by axisymmetric Stokes equations. Taking into account the fact that the jet is thin and long, we used slender body theory to obtain the solution of the Stokes equations. We find that the presence of surfactant has a significant effect on the system and retards the pinch-off, i.e., the breakup of the jet. The influence of surfactant on the jet deformation and breakup is also studied at different Peclet numbers, i.e., for different ratios between convection and diffusion of surfactant. It is found that diffusion of surfactant causes the jet to pinch faster. At larger values of Peclet number ($Pe_s = 1000$), first the pinching is delayed with the formation of a filament, but eventually it pinches. We also considered the effect of different relationships between the surfactant concentration

and interfacial tension. We considered linear as well as non-linear relationships between surface tension and surfactant concentration. It is found that the equation of state does not have much effect on the necking. We also generalize these results to consider the case of a slightly viscous jet in highly viscous fluid. It is found that the pinch-off occurs at a different location, which has a consequences concerning the satellite drop formation.

We also performed experiments, which support the predictions of the model. On the experimental front, we used high speed digital camera to capture the details of the pinching jet. Air bubbles in a glycerol/water mixture are created for both with and without surfactant. Digitized video images of the bubble elongation were captured sequentially in time and analyzed using image analysis software. It is found that the presence of surfactant slows down the breakup of a slightly viscous jet in a highly viscous exterior fluid.

CHAPTER 2

MATHEMATICAL MODELS

In this chapter, the basic hydrodynamic equations and boundary conditions are formulated. We consider Stokes equations to model the flow outside the jet and derive boundary conditions at the interface for the clean surface (i.e., no surfactant). The boundary conditions are then modified to take into account the presence of surfactant. We consider the case of insoluble surfactant and use a convection diffusion equation for the transport of surfactant along the interface.

2.1 Stokes Flow

The Navier-Stokes equations describe the flow field of a fluid at any point in the domain in terms of $\mathbf{u}$ and p, the velocity and pressure of the fluid respectively. They are given by

$$\rho\frac{\partial \mathbf{u}}{\partial t} + \rho(\mathbf{u}\cdot\nabla)\mathbf{u} = -\nabla p + \mu\nabla^2\mathbf{u}, \tag{2.1}$$

where ρ is the density of the fluid and μ is the viscosity. In order to non-dimensionalize the above equation, we define the following non-dimensional quantities

$$\widetilde{\mathbf{u}} = \frac{\mu}{\sigma_o}\mathbf{u}, \quad \widetilde{\mathbf{x}} = \frac{\mathbf{x}}{L}, \quad \widetilde{p} = \frac{L}{\sigma_o}p, \quad \widetilde{t} = \frac{\sigma_o}{\mu B}t. \tag{2.2}$$

The non-dimensional form of Equation (2.1)(without tildes) is

$$\frac{\partial \mathbf{u}}{\partial t} + (\mathbf{u}\cdot\nabla)\mathbf{u} = \frac{1}{Re}[-\nabla p + \nabla^2\mathbf{u}], \tag{2.3}$$

where $Re = \frac{\rho\sigma_o L}{\mu^2}$ is called the Reynolds number, and it represents the ratio of the inertial and viscous forces. For the case of slow flow or Stokes flow it is assumed that

the viscous terms are more dominant as compared to the inertial terms so $Re \ll 1$. Equations (2.3) simplify to

$$-\nabla p + \nabla^2 \mathbf{u} = 0. \tag{2.4}$$

Rewriting

$$\nabla^2 \mathbf{u} = \nabla p. \tag{2.5}$$

These equations are known as Stokes equations. The linear nature of the Stokes equations allows us to build an extensive theoretical framework regarding the mathematical properties of the solutions and physical nature of the flow [27]. In addition, for incompressible fluid we have the continuity equation

$$\nabla \cdot \mathbf{u} = 0. \tag{2.6}$$

In these kind of flows, pressure and viscous forces are in equilibrium throughout the fluid at each instant. Thus, even though the flow may be time dependent, the temporal variables do not appear in the governing equations.

2.2 Flow Domain and Governing Equations

In this section, we present the flow geometry and derive governing equations in dimensional form. We consider an infinite, axisymmetric, periodic fluid jet surrounded by another viscous fluid. The jet is assumed to be slender, i.e., the wavelength of the jet is much greater than its average width. Alternatively, one may consider a long slender fluid droplet immersed in a viscous fluid. Initially, we consider the interior of the jet to be inviscid, we can think of it as an analogue of a long air bubble. The jet is assumed to be axisymmetric with respect to the axial coordinate axis, which corresponds to the axis of symmetry. The surrounding fluid is assumed to be viscous, incompressible and Newtonian. Neglecting inertia, the governing equations

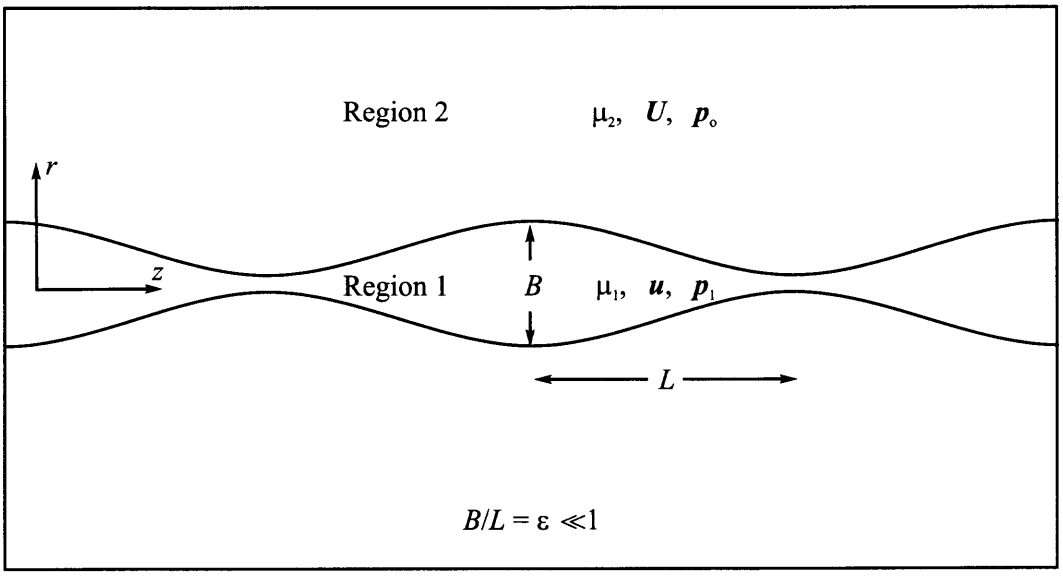

Figure 2.1 Schematic diagram of flow geometry.

in the jet exterior are axisymmetric Stokes equations and the continuity equation. Considering a cylindrical coordinate system (r, θ, z), the surface of the jet is denoted by $r = R(z,t)$ and the axial and radial components of the velocity are u_z and u_r respectively. Governing equations for the outer fluid are the Stokes equations

$$\mu\left(\frac{1}{r}\frac{\partial}{\partial r}(r\frac{\partial u_z}{\partial r}) + \frac{\partial^2 u_z}{\partial z^2}\right) = \frac{\partial p}{\partial z}, \tag{2.7}$$

$$\mu\left(\frac{1}{r}\frac{\partial}{\partial r}(r\frac{\partial u_r}{\partial r}) - \frac{u_r}{r^2} + \frac{\partial^2 u_r}{\partial z^2}\right) = \frac{\partial p}{\partial r}. \tag{2.8}$$

The continuity equation is

$$\frac{\partial u_z}{\partial z} + \frac{1}{r}\frac{\partial}{\partial r}(ru_r) = 0. \tag{2.9}$$

2.3 Boundary Conditions: Clean Flow

Boundary conditions for our problem are prescribed at the interface between the two phases. These boundary conditions are the continuity of the tangential stress and a jump in the normal stress at the interface [9].

Tangential stress balance:

$$t_i S_{ij} n_j = 0, \quad \text{at } r = \tilde{R}(z,t), \tag{2.10}$$

where

$$S_{ij} = \frac{\mu}{2}\left(\frac{\partial u_i}{\partial x_j} + \frac{\partial u_j}{\partial x_i}\right)$$

is the stress tensor written in Cartesian form, t_i are the components of a unit tangent t and n_i are the components of a unit outward normal evaluated at interface. In terms of cylindrical coordinate system, equation (2.10) becomes

$$\frac{2\mu}{(1+R'^2)}\left[R'\frac{\partial u_r}{\partial r} + (1-R'^2)\frac{1}{2}(\partial u_r \partial z + \frac{\partial u_z}{\partial r}) - R'\frac{\partial u_z}{\partial z}\right] = 0, \quad \text{at } r = \tilde{R}(z,t), \tag{2.11}$$

where primes denote $\frac{\partial}{\partial z}$.

Normal stress balance:

$$n_i S_{ij} n_j = \sigma_o \kappa, \quad \text{at } r = \tilde{R}(z,t).$$

In terms of cylindrical coordinates, the normal stress balance reads

$$p_i - p_o + \frac{2\mu}{(1+R'^2)}\left[\frac{\partial u_r}{\partial r} - R'(\frac{\partial u_r}{\partial z} + \frac{\partial u_z}{\partial r}) + R'^2\frac{\partial u_z}{\partial z}\right] = \frac{\sigma_o}{R\sqrt{1+R'^2}}[1 - \frac{RR''}{1+R'^2}], \tag{2.12}$$

where

σ_o= surface tension of the clean interface,

p_i = inside pressure,

p_o = outside pressure,

κ = mean interfacial curvature.

Kinematic boundary condition:

Kinematics condition at the interface states that no fluid particle crosses the interface, i.e., if a particle is at the interface it remains at the interface. In cylindrical coordinate system, kinematic condition at the interface is given by

$$u_r = \frac{\partial R}{\partial t} + u_z \frac{\partial R}{\partial z}, \quad \text{at } r = \tilde{R}(z,t). \tag{2.13}$$

2.4 Boundary Conditions: With Surfactant

Surfactants are chemical species which align themselves at the interface and alter the interfacial properties. The surface tension, now denoted by $\sigma(\Gamma)$, is a function of surfactant concentration Γ. The precise nature of the functional dependance is discussed in Section 2.5. The effect of the surfactant is incorporated into the mathematical model by modifying the stress conditions. The presence of surfactant introduces a tangential interfacial force which is proportional to the surface tension gradient [9]. This added force term is present in the tangential stress balance condition.

Tangential stress balance incorporating surfactant:

$$t_i S_{ij} n_j = -\nabla\sigma(\Gamma) \cdot t, \quad \text{at } r = \tilde{R}(z,t), \tag{2.14}$$

where

$$S_{ij} = \frac{\mu}{2}\left(\frac{\partial u_i}{\partial x_j} + \frac{\partial u_j}{\partial x_i}\right),$$

is the stress tensor written in Cartesian form, t_i are the components of a unit tangent t and n_i are the components of a unit outward normal evaluated at interface and $\sigma(\Gamma)$ represents the variable surface tension that changes with surfactant concentration.

In terms of cylindrical coordinate system, we get

$$\frac{2\mu}{(1+R'^2)}\left[R'\frac{\partial u_r}{\partial r} + (1-R'^2)\frac{1}{2}\left(\frac{\partial u_r}{\partial z} + \frac{\partial u_z}{\partial r}\right) - R'\frac{\partial u_z}{\partial z}\right] = -\frac{\partial\sigma}{\partial z}\frac{1}{\sqrt{1+R'^2}}. \tag{2.15}$$

Normal stress balance incorporating surfactant:

$$n_i S_{ij} n_j = \sigma(\Gamma)\kappa, \quad \text{at } r = \tilde{R}(z,t).$$

In terms of cylindrical coordinates, the normal stress balance reads

$$p_i - p_o + \frac{2\mu}{(1+R'^2)}\left[\frac{\partial u_r}{\partial r} - R'\left(\frac{\partial u_r}{\partial z} + \frac{\partial u_z}{\partial r}\right) + R'^2\frac{\partial u_z}{\partial z}\right] = \frac{\sigma(\Gamma)}{R\sqrt{1+R'^2}}\left[1 - \frac{RR''}{1+R'^2}\right]. \tag{2.16}$$

2.5 Relationship Between Surface Tension and Surfactant Concentration

The total amount of surfactant is constant at the interface and the surface tension is a decreasing function of the surfactant concentration. The relationship between the surface tension and the surfactant concentration is given by the equation of state $\sigma = \sigma(\Gamma)$. These are determined empirically, there are several different kinds of relationships which are used. The simplest model for the dependance of interfacial tension σ on a surfactant concentration Γ is given by the linear relationship [34]

$$\sigma = \sigma_o - TR\Gamma, \tag{2.17}$$

where σ_o is the surface tension of the clean interface, T is the absolute temperature, R is the universal gas constant and Γ_o is the uniform surfactant concentration of the unperturbed interface. Typically, such a relationship is valid for dilute surfactant concentration. In some situations, such as in the case of contracting interfaces, the surfactant concentration may become large at some points. In these situations, a more precise model with a non-linear dependance of σ on Γ is used. Although there are different forms of non-linear equation of state used in literature, the most commonly used is the so called Langmuir equation [9]

$$\sigma = \sigma_o + (RT\Gamma_\infty)\ln\left(1 - \frac{\Gamma}{\Gamma_\infty}\right), \tag{2.18}$$

where σ_o is the surface tension of the clean interface, Γ_∞ is the maximum allowable interfacial concentration of the surfactant (the maximum packing density), R is the universal gas constant and T is the absolute temperature.

2.6 Surfactant Transport

In order to quantify the effect of surfactant on the interface, we introduce a convection diffusion equation which governs the surfactant transport along the interface. The presence of exterior fluid causes the surfactant to spread across the interface in a non-uniform way. There are other factors as well that might influence the surfactant distribution such as diffusion and the evolution of the interface (e.g., stretching or contracting).

Stone [33] presented a simple derivation of time dependent equation for surfactant transport along a deforming interface

$$\left.\frac{\partial \Gamma}{\partial t}\right|_s + \nabla_s \cdot (\Gamma \mathbf{u}_s) - D_s \nabla_s^2 \Gamma + \Gamma \kappa \mathbf{u} \cdot \mathbf{n} = 0, \tag{2.19}$$

where Γ is the surfactant concentration, $\frac{\partial}{\partial t}|_s$ denotes the time derivative keeping the arc length coordinate fixed, $\nabla_s = (\mathbf{I} - \mathbf{nn}) \cdot \nabla$ is the surface gradient operator, $\mathbf{u}_s$ is the velocity at the interface, κ is the mean curvature of the interface and D_s is the interfacial surfactant diffusivity.

Wong, Rumschitzki and Maldarelli [40] suggested a modified equation for other parametrizations of the interface (i.e., not necessarily arc length). With the tools of differential geometry, they show that it is necessary to include an additional term to incorporate the effect of the changing Lagrangian coordinate system. The modified equation is

$$\left.\frac{\partial \Gamma}{\partial t}\right|_\alpha - \frac{\partial \mathbf{X}}{\partial t} \cdot \nabla_s \Gamma + \nabla_s \cdot (\Gamma \mathbf{u}_s) - D_s \nabla_s^2 \Gamma + \Gamma \kappa \mathbf{u} \cdot \mathbf{n} = 0, \tag{2.20}$$

where $\mathbf{X}(\alpha, t)$ is a parametric representation of the interface and all the other parameters have the meanings defined above. In this study, we have considered the surfactant to be insoluble, i.e., there is no net flux of the surfactant to and from the interface to the bulk fluid.

CHAPTER 3

BREAKUP OF INVISCID JET IN VISCOUS SURROUNDING IN PRESENCE OF INSOLUBLE SURFACTANT

In this chapter, we use long wavelength asymptotics to derive governing equations for the evolution of the jet interface and surfactant concentration. We first consider the effect of surfactant on the breakup of an inviscid jet in highly viscous exterior fluid. A more general case of a slightly viscous jet will be considered later. These long wave equations are studied both analytically and numerically to investigate the influence of surfactant on the pinch-off process. Different physical effects are also incorporated into the model and the results are discussed.

3.1 Non-Dimensionalization

We introduce the axial length scale L to be the wavelength of the jet and define B to be the radial distance to the surface of the undisturbed jet. Also define Γ_o to be the uniform surfactant concentration for the undisturbed jet. We non-dimensionalize the differential equations and boundary conditions by introducing the following dimensionless variables

$z' = \frac{z}{L}$, $r' = \frac{r}{L}$, $u' = \frac{\mu}{\sigma_o}u$, $t' = \frac{\sigma_o}{\mu B}t$, $\Gamma' = \frac{\Gamma}{\Gamma_o}$, $p'_o = \frac{L}{\sigma_o}p_o$, $p'_i = \frac{B}{\sigma_o}p_i$, $\epsilon = B/L$.

Substituting into the Stokes equations and the interfacial boundary conditions (dropping primes), we get the following system of dimensionless equations and boundary conditions:

$$\frac{1}{r}\frac{\partial}{\partial r}(r\frac{\partial u_z}{\partial r}) + \frac{\partial^2 u_z}{\partial z^2} = \frac{\partial p_o}{\partial z}, \tag{3.1}$$

$$\frac{1}{r}\frac{\partial}{\partial r}(r\frac{\partial u_r}{\partial r}) - \frac{u_r}{r^2} + \frac{\partial^2 u_r}{\partial z^2} = \frac{\partial p_o}{\partial r}. \tag{3.2}$$

The continuity equation becomes

$$\frac{\partial u_z}{\partial z} + \frac{1}{r}\frac{\partial}{\partial r}(ru_r) = 0. \tag{3.3}$$

The non-dimensional tangential stress balance, normal stress balance and the kinematic condition evaluated at the interface $r = \epsilon R(z,t)$ are given by

$$\frac{2}{(1+\epsilon^2 R'^2)}\left[\epsilon R'\frac{\partial u_r}{\partial r} + (1-\epsilon^2 R'^2)\frac{1}{2}(\frac{\partial u_r}{\partial z} + \frac{\partial u_z}{\partial r}) - \epsilon R'\frac{\partial u_z}{\partial z}\right] = -\frac{\partial \sigma}{\partial z}\frac{1}{\sqrt{1+\epsilon^2 R'^2}}, \tag{3.4}$$

$$p_i - \epsilon p_o + \frac{2\epsilon}{(1+\epsilon^2 R'^2)}\left[\frac{\partial u_r}{\partial r} - \epsilon R'(\frac{\partial u_r}{\partial z} + \frac{\partial u_z}{\partial r}) + \epsilon^2 R'^2\frac{\partial u_z}{\partial z}\right] = \frac{\sigma}{R\sqrt{1+\epsilon^2 R'^2}}\left[1 - \frac{\epsilon^2 RR''}{1+\epsilon^2 R'^2}\right], \tag{3.5}$$

$$u_r = R_t + \epsilon R' u_z. \tag{3.6}$$

The non-dimensional surfactant transport equation is given by

$$\frac{\partial \Gamma}{\partial t} + \frac{\epsilon}{R\sqrt{1+\epsilon^2 R'^2}}\frac{\partial}{\partial z}\left[\frac{R\Gamma}{\sqrt{1+\epsilon^2 R'^2}}(\epsilon u_r R' + u_z)\right] - \frac{\epsilon^2 R'}{1+\epsilon^2 R'^2}\frac{\partial R}{\partial t}\frac{\partial \Gamma}{\partial z} \tag{3.7}$$
$$-\frac{\epsilon}{Pe_s}\left[\frac{1}{R\sqrt{1+\epsilon^2 R'^2}}\frac{\partial}{\partial z}(\frac{R}{\sqrt{1+\epsilon^2 R'^2}}\frac{\partial \Gamma}{\partial z})\right] + \frac{\Gamma(u_r - \epsilon R' u_z)}{R(1+\epsilon^2 R'^2)}[1 - \frac{\epsilon^2 RR''}{1+\epsilon^2 R'^2}] = 0,$$

where we have introduced a surface Peclet number $Pe_s = \frac{\sigma_o L}{D_s \mu}$. In non-dimensional form, the linearized equation of state relating surfactant concentration Γ to the surface tension σ, takes the form

$$\sigma = 1 - \beta\Gamma, \tag{3.8}$$

where $\beta = \frac{RT\Gamma_o}{\sigma_o}$. This parameter is called the sensitivity parameter and it measures the sensitivity of the surface tension to the surfactant concentration.

3.2 Method of Solution

Flow exterior to the jet is governed by the Stokes equations and continuity equation given by

$$\nabla p_o = \nabla^2 \mathbf{u}, \tag{3.9}$$

$$\nabla \cdot \mathbf{u} = 0,$$

where $\mathbf{u}$ is the velocity field and p_o is the pressure field. To find the solution of the above system, we use an approach based upon the fundamental solution of the Stokes equations. An exact solution of the Stokes equations can be written as the integral of a distribution of point forces, or Stokeslets, over the boundary of the fluid region; this result holds for both rigid and deformable boundaries. For the case of slender bodies and the objects with small aspect ratio, we can approximate the outside flow by replacing the distribution of the point forces on its boundary by a distribution of point forces and other singularities along the centerline of the body.

If the slender body is deformable, as in our case, the singularities required to satisfy the boundary conditions to the leading order are point mass sources and point forces (Stokeslets) alone [4]. The representation of the flow field due to the distribution of $f(\bar{z})$ of Stokeslets and $g(\bar{z})$ of point sources, becomes (in non-dimensional form)

$$u_r \sim r \int_{-1}^{1} \left(\frac{f(\bar{z})(z-\bar{z})}{S^3} + \frac{g(\bar{z})}{S^3} \right) d\bar{z}, \tag{3.10}$$

$$u_z \sim \int_{-1}^{1} \left(\frac{f(\bar{z})}{S} + \frac{f(\bar{z})(z-\bar{z})^2}{S^3} + \frac{g(\bar{z})(z-\bar{z})}{S^3} \right) d\bar{z}, \tag{3.11}$$

$$p_o \sim 2 \int_{-1}^{1} \frac{f(\bar{z})(z-\bar{z})}{S^3} d\bar{z}, \tag{3.12}$$

where $f(\bar{z})$ and $g(\bar{z})$ are the densities of the Stokeslets and sources respectively and

$$S = [(z-\bar{z})^2 + r^2)]^{\frac{1}{2}}.$$

The strength of the Stokeslets and point sources $f(\overline{z})$ and $g(\overline{z})$ are unknowns and must be determined subject to the boundary conditions.

3.3 Asymptotic Analysis

We note that our equations and boundary conditions involve the quantities, u_r, u_z, p, $\frac{\partial u_r}{\partial z}$, $(\frac{\partial u_r}{\partial z} + \frac{\partial u_z}{\partial r})$ etc. at the interface. These quantities involve the integrals over the source and Stokeslet densities and may be localized by evaluating the leading order contribution using the method given in Handelsman and Keller [13]. It is simpler to describe the method for a finite jet with $-1 \leq z \leq 1$, although later on we shall apply the result to study the pinch-off of a periodic jet.

The main idea is to expand $f(\overline{z})$ and $g(\overline{z})$ in a Taylor series about z, e.g.,

$$\begin{aligned} f(\overline{z}) &= f(z) + f'(z)(\overline{z} - z) + f''(z)\frac{(z-\overline{z})^2}{2!} + R_f, \\ g(\overline{z}) &= g(z) + g'(z)(\overline{z} - z) + g''(z)\frac{(z-\overline{z})^2}{2!} + R_g, \end{aligned} \tag{3.13}$$

where R_f and R_g denote the remainder terms in the Taylor series expansions.

Substitute the above expansions in (3.10), (3.11), (3.12) and integrate the resulting expressions analytically to calculate the leading order contribution. In order to explain the whole procedure, we present a detailed analysis for one integral. Recall that to leading order

$$u_r = r\int_{-1}^{1}\left(\frac{f(\overline{z})(z-\overline{z})}{S^3} + \frac{g(\overline{z})}{S^3}\right)d\overline{z}. \tag{3.14}$$

If we put the expressions for $f(\overline{z})$ and $g(\overline{z})$ in the integral, we get the following exact representation of (3.14)

$$\begin{aligned} u_r = r\int_{-1}^{1}\frac{f(z)(z-\overline{z})}{S^3}d\overline{z} - r\int_{-1}^{1}\frac{f'(z)(z-\overline{z})^2}{S^3}d\overline{z} + r\int_{-1}^{1}\frac{R_f(z-\overline{z})}{S^3}d\overline{z} \\ + r\int_{-1}^{1}\frac{g(z)}{S^3}d\overline{z} + r\int_{-1}^{1}\frac{g'(z)(z-\overline{z})}{S^3}d\overline{z} \\ + r\int_{-1}^{1}\frac{g''(z)(z-\overline{z})^2}{S^3}d\overline{z} + r\int_{-1}^{1}\frac{R_g}{S^3}d\overline{z}. \end{aligned} \tag{3.15}$$

Note that the integrands of the remainder terms (third and the seventh terms above) are bounded. Hence, the remainder terms are $O(\epsilon f, \epsilon g)$, when evaluated at the interface $r = \epsilon R$.

We can write the above equation as

$$u_r = I_1 - I_2 + I_3 + I_4 + I_5 + O(\epsilon f, \epsilon g), \tag{3.16}$$

where each of the intergals $I_i, (i = 1, ..., 5)$ can be performed exactly; for example

$$I_1 = r \int_{-1}^{1} \frac{f(z)(z - \overline{z})}{S^3} d\overline{z} = \frac{f(z)r}{\sqrt{r^2 + (z-1)^2}} - \frac{f(z)r}{\sqrt{r^2 + (z+1)^2}}. \tag{3.17}$$

At $r = \epsilon R$, we have

$$I_1 = f(z)\left[\frac{\epsilon R}{\sqrt{(\epsilon R)^2 + (z-1)^2}} - \frac{\epsilon R}{\sqrt{(\epsilon R)^2 + (z+1)^2}}\right].$$

For $\epsilon \ll 1$ and z far enough from the bubble endpoints,

$$I_1 = \frac{\epsilon R f(z)}{(z-1)}\left[1 - \frac{1}{2}\frac{(\epsilon R)^2}{(z-1)}\right] - \frac{\epsilon R f(z)}{(z+1)}\left[1 - \frac{1}{2}\frac{(\epsilon R)^2}{(z+1)}\right],$$

so that

$$I_1 \sim O(\epsilon f). \tag{3.18}$$

Similarly,

$$I_2 = r \int_{-1}^{1} \frac{f'(z)(z - \overline{z})^2}{S^3} d\overline{z}, \tag{3.19}$$

$$I_2 = \left[\frac{z-1}{\sqrt{r^2 + (z-1)^2}} - \frac{z+1}{\sqrt{r^2 + (z+1)^2}} - \ln(z - 1 + \sqrt{r^2 + (z-1)^2}) \right.$$
$$\left. + \ln(z + 1 + \sqrt{r^2 + (z+1)^2})\right] r f'(z). \tag{3.20}$$

Substituting $r = \epsilon R$, expanding for small ϵ and taking the leading order contributions, we get

$$I_2 \sim 2(\epsilon R) f' \ln \frac{1}{\epsilon R}. \tag{3.21}$$

Next, we evaluate

$$I_3 = r \int_{-1}^{1} \frac{g(z)}{S^3} d\bar{z} = \frac{r(z-1)g(z)}{r^2\sqrt{r^2+(z-1)^2}} - \frac{r(-z-1)g(z)}{r^2\sqrt{r^2+(z+1)^2}}, \tag{3.22}$$

which for $r = \epsilon R$ and $\epsilon \ll 1$ gives

$$I_3 \sim \frac{2g}{\epsilon R}. \tag{3.23}$$

Similarly, the remaining integrals can be evaluated approximately to the leading order and we get

$$I_4 \sim O(\epsilon g). \tag{3.24}$$

Also,

$$I_5 \sim -2(\epsilon R) g'' \ln \frac{1}{\epsilon R}. \tag{3.25}$$

Putting all the values of I_1, I_2, I_3, I_4 and I_5 in (3.16), we get an expression for the radial component of the velocity up to the leading order in f and g

$$u_r \sim -2\epsilon R f' \ln \frac{1}{\epsilon R} + \frac{2g}{\epsilon R}. \tag{3.26}$$

Similarly, putting the expansions for $f(\bar{z})$ and $g(\bar{z})$ in the integrals for u_z and p_o and evaluating the integrals as before up to leading order in f and g, we get the following expressions

$$u_z \sim 4f \ln \frac{1}{\epsilon R} - 2g' \ln \frac{1}{\epsilon R}, \tag{3.27}$$

$$p_o \sim -4f' \ln \frac{1}{\epsilon R}. \tag{3.28}$$

Expressions for the derivatives of the velocity that appear in the stress balance conditions are obtained by differentiating (3.10) and (3.11). After localizing as above, we obtain (to leading order)

$$\frac{\partial u_r}{\partial r} \sim -2f' \ln \frac{1}{\epsilon R} - 2g \frac{1}{\epsilon^2 R^2}, \tag{3.29}$$

$$\frac{\partial u_z}{\partial z} \sim 4f' \ln \frac{1}{\epsilon R} - 2g'' \ln \frac{1}{\epsilon R}, \tag{3.30}$$

$$\frac{\partial u_r}{\partial z} + \frac{\partial u_z}{\partial r} \sim -4f \frac{1}{\epsilon R} + 4g' \frac{1}{\epsilon R}. \tag{3.31}$$

Remarks:

Near the bubble end points the above analysis breaks down. Since we are mainly interested in deriving local equations describing bubble evolution and pinch-off away from endpoints, this is not a major difficulty. Modifications of the method which can provide leading order expressions near the bubble endpoints are discussed by Handelsman and Keller [13]. In this study, we are studying an infinite periodic jet, so the integrals given in (3.10)-(3.11) have a range from $-\infty$ to $+\infty$. For example, the expression for u_r can be written as

$$u_r = \int_{-\infty}^{-1} \left(\frac{f(\overline{z})(z-\overline{z})}{S^3} + \frac{g(\overline{z})}{S^3} \right) d\overline{z} + \int_{-1}^{1} \left(\frac{f(\overline{z})(z-\overline{z})}{S^3} + \frac{g(\overline{z})}{S^3} \right) d\overline{z} + \int_{1}^{+\infty} \left(\frac{f(\overline{z})(z-\overline{z})}{S^3} + \frac{g(\overline{z})}{S^3} \right) d\overline{z}.$$

Since these integrals are singular at $z = \bar{z}$ in the limit $r \to 0$, the major contribution arises from the middle integral and the first and the third integrals converge.

We use the expressions (3.29) to (3.31) in the equations for the tangential stress balance, normal stress balance, kinematic condition and the equation for the surfactant transport. In the following, we equate the leading order terms in tangential stress balance, normal stress balance and kinematic condition to obtain expressions for f and g.

First, collecting the leading order terms in the tangential stress balance, we get

$$-\frac{4f}{\epsilon R} - \frac{4gR'}{\epsilon R^2} + \frac{4g'}{\epsilon R} = \beta\Gamma_z. \tag{3.32}$$

This equation suggests that f and g are of the same order. Keeping the leading order terms in f and g in the normal stress balance gives

$$p_i - 4\epsilon f' \ln\frac{1}{\epsilon R} - \frac{4g}{\epsilon R^2} = \frac{\sigma}{R}. \tag{3.33}$$

Under the assumption that f and g are of the same order, to leading order equation (3.33) takes the form

$$p_i - \frac{4g}{\epsilon R^2} = \frac{\sigma}{R}. \tag{3.34}$$

We conclude that g must be of $O(\epsilon)$ for the above equality to hold. Hence, we can write

$$g = \epsilon g_0, \tag{3.35}$$

$$f = \epsilon f_0, \tag{3.36}$$

where $g_0 = O(1)$ and $f_0 = O(1)$. Using (3.34) and (3.35), we can write the leading order normal stress balance as

$$p_i - \frac{4g_0}{R^2} = \frac{\sigma}{R}. \tag{3.37}$$

We can solve equation (3.37) for g_0 to get

$$g_0 = \frac{R}{4}(Rp_i - \sigma). \tag{3.38}$$

Note that (3.32) now gives an expression for the Stokeslet density f in terms of R, p_i and Γ, although f decouples from the other leading order equations.

The leading order contribution from the kinematic condition is

$$\frac{2g_0}{R} = R_t. \tag{3.39}$$

Putting (3.38) in (3.39), we get an equation which governs the interface of a slender, axisymmetric and inviscid jet in the presence of surfactant at the interface

$$R_t = \frac{1}{2}(p_i R - \sigma). \tag{3.40}$$

The leading order surfactant transport equation is obtained by substituting (3.26), (3.27), (3.35), (3.36) into the surfactant transport equation (3.7) with the result

$$\frac{\partial \Gamma}{\partial t} + \frac{2\Gamma g_0}{R^2} = 0. \tag{3.41}$$

Putting the value of g_0 from (3.38) into (3.41), we get an equation for the evolution of the surfactant concentration Γ given by

$$\frac{\partial \Gamma}{\partial t} + \frac{\Gamma}{2R}(Rp_i - \sigma) = 0. \tag{3.42}$$

Hence, the leading order governing equations for our system, i.e., the evolution equation for the jet interface and surfactant concentration are given by

$$\frac{\partial R}{\partial t} = \frac{1}{2}(Rp_i + \beta\Gamma - 1), \tag{3.43}$$

$$\frac{\partial \Gamma}{\partial t} = -\frac{\Gamma}{2R}(Rp_i + \beta\Gamma - 1), \tag{3.44}$$

where we have substituted $\sigma = 1 - \beta\Gamma$, the linearized equation of state relating the surface tension and the surfactant concentration.

3.4 Derivation of Inside Pressure

In our system of governing equations, we still have to calculate the inside pressure p_i. For this, we use the constant volume assumption, which in non-dimensional form is given by

$$\int_{-1}^{1} R^2 dz = 2. \tag{3.45}$$

Therefore,

$$\frac{d}{dt}\int_{-1}^{1} R^2 dz = 0,$$

so that

$$\int_{-1}^{1} 2RR_t dz = 0$$

Recall that the value of R_t is given by

$$R_t = \frac{1}{2}(p_i R - \sigma).$$

Using the value of R_t, we get

$$\int_{-1}^{1} p_i R^2 dz - \int_{-1}^{1} \sigma R dz = 0. \tag{3.46}$$

Finally, using (3.45) in (3.46), our expression for the inside pressure reduces to

$$p_i = \frac{1}{2}\int_{-1}^{1} \sigma R dz. \tag{3.47}$$

Equations (3.43), (3.44) and (3.47) are the desired long wave evolution equations which govern the dynamics of an inviscid, axisymmetric and periodic fluid jet in presence of insoluble surfactant.

Before we solve these long wave equations numerically, we observe that an important result follows immediately from (3.43) and (3.44). If we divide (3.43) by R, (3.44) by Γ and add the resulting equations, we get

$$\frac{R_t}{R} + \frac{\Gamma_t}{\Gamma} = 0, \tag{3.48}$$

which can be solved to give

$$\Gamma = \frac{C(z)}{R}, \tag{3.49}$$

where $C(z)$ is a constant of integration and depends only on initial conditions. It can be concluded that pinch-off (i.e., $R \to 0$, for some z) can only occur if $\Gamma \to \infty$. In

this case, our model using a linear or non-linear equation of state breaks down since σ will become negative. Nevertheless this feature combined with the form of equation (3.44) suggests that $R \rightarrow 0$ will not occur.

3.5 Numerical Solution

In order to investigate the non-linear evolution of the long wave equations, we numerically solve the coupled non-linear system of partial differential equations governing the evolution of the interface $R(z,t)$ and surfactant concentration $\Gamma(z,t)$. Recall that the governing equations are

$$\frac{\partial \Gamma}{\partial t} = -\frac{\Gamma}{2R}(Rp_i + \beta\Gamma - 1), \tag{3.50}$$

$$\frac{\partial R}{\partial t} = \frac{1}{2}(Rp_i + \beta\Gamma - 1), \tag{3.51}$$

$$p_i = \frac{1}{2}\int_{-1}^{1}[1 - \beta\Gamma]Rdz, \tag{3.52}$$

We use the method of lines employing a Runge-Kutta integrator to solve the above coupled system. Here note that the inside pressure is a function of time only and is given by the global condition (3.52). We use trapezoidal rule to evaluate the integral, which is then used in the evolution equations to get the surfactant concentration and the jet radius. As an initial condition, we used $\Gamma = 1$, and $R = a + bcos\pi z$. We have conservation of volume and conservation of surfactant as two conserved quantities in our system given by

$$\int_{-1}^{1} R^2 dz = 2, \tag{3.53}$$

$$\int_{-1}^{1} \Gamma R dz = 2. \tag{3.54}$$

These quantities are conserved in our numerical simulations within $10^{-5} - 10^{-6}$, which are used as a check to the accuracy of our calculations.

Figure 3.1 shows the results for the jet radius in the case of a clean interface. The solution is plotted at various time steps. It is observed that in the case of no surfactant, the jet profile is parabolic all the way to the pinch-off, as was observed in the studies of Doshi et al. [8]. We note that without surfactant the jet radius becomes zero, i.e., pinch-off occurs in finite time. On the other hand, Figure 3.2 shows the jet radius in the presence of surfactant. We see that the presence of surfactant retards the pinch-off and a finite time singularity, which was observed in the case of no surfactant is inhibited. In stead of pinch-off, we observe the formation of a thin and long filament. Figure 3.3 represents the surfactant concentration at different time steps. It shows that the surfactant concentration is high in the neck region. Since the total amount of surfactant is conserved, as the surface area decreases, the amount of surfactant increases. This dramatically decreases the surface tension in the neck and hence makes the filament less susceptible to the surface tension driven instability. Moreover this high value of surfactant concentration in the filament also suggests to choose a non-linear equation of state, which is appropriate for low as well as high surfactant concentrations.

The evolution shown in Figure 3.2 does not exhibit a trend suggesting that the interface will pinch-off in finite time. Instead, steep gradients develop at large times in the simulations. Additional physical effects, in this simplified model can become important when large interfacial gradients develop. Two physical effects that were neglected in the present model are the Marangoni effects and the surface diffusion of surfactant. In Section 3.7, we will consider the influence of Marangoni forces and surface diffusion of surfactant on the interfacial dynamics, and in particular, whether these inclusions can lead to pinch-off of the interface.

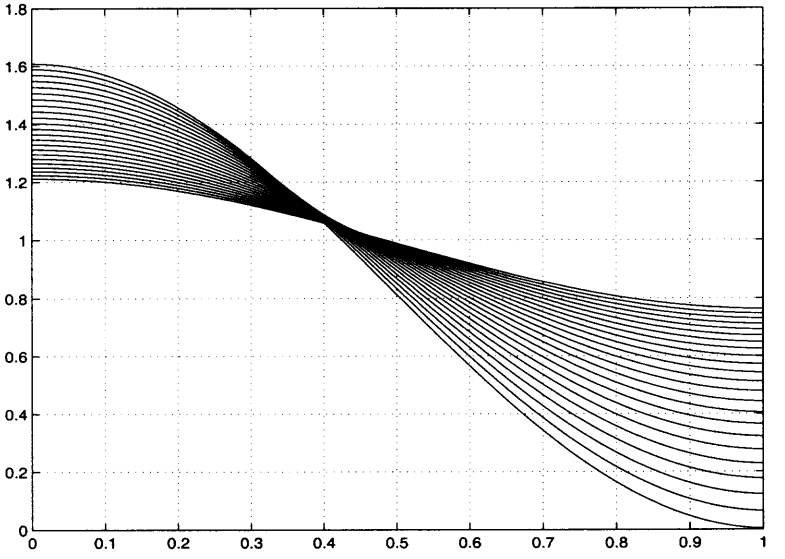

Figure 3.1 Jet radius R vs axial direction z for clean interface.

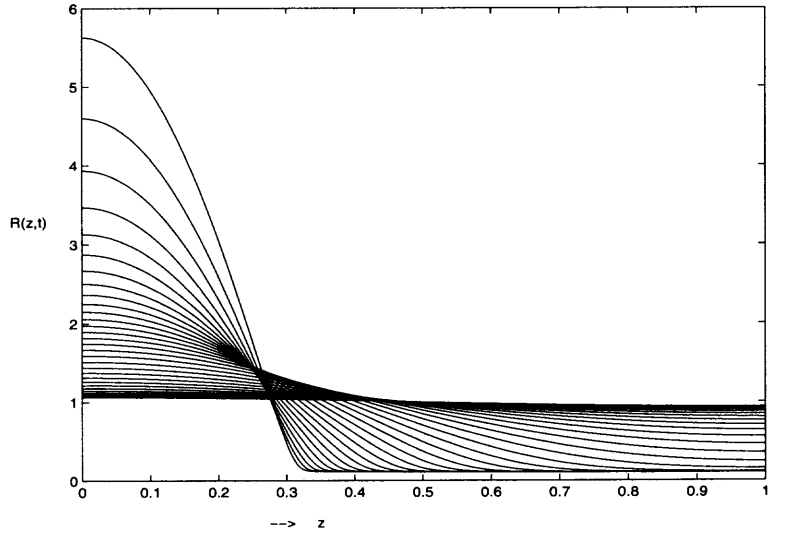

Figure 3.2 Jet radius R vs axial direction z in presence of surfactant.

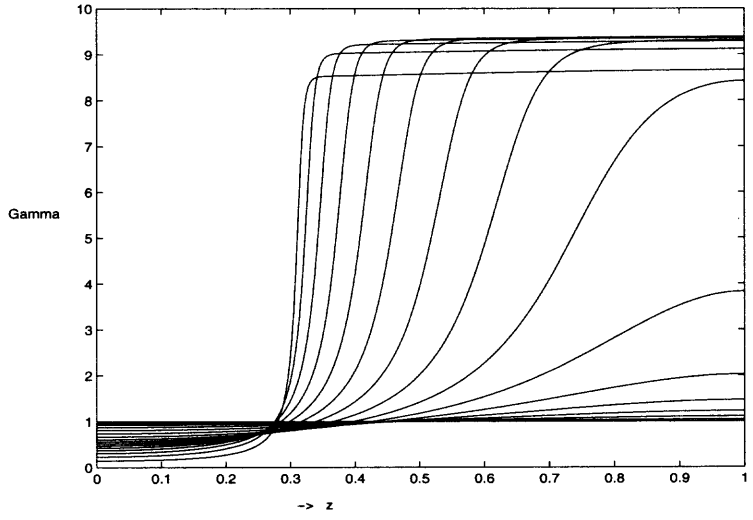

Figure 3.3 Surfactant concentration.

3.6 Comparison with Full Numerical Simulations

In this section, we compare the results of the long wavelength model with the full numerical simulations of the Navier-Stokes equation for the case of an inviscid jet. This work is done in collaboration with J. Lie and Y. Young. We numerically investigate the breakup of an inviscid jet, suspended in a viscous exterior fluid in the presence of an insoluble surfactant at the interface using a moving grid method. A boundary-fitted coordinate system is used in which the free surface coincides with one line of the numerical grid.

Figure 3.4 shows the evolution of a slender inviscid bubble in viscous exterior fluid. The dotted lines show the initial bubble shape and the thick line is the final evolved shape. We see that during the evolution of the jet interface, the presence of surfactant retards the pinch-off and a thin and long filament is formed. The numerical simulations of the long wave model just show this type of effect. Marangoni terms do not appear in the long wavelength model. From the full simulations, we see that the Marangoni terms are not important close the pinch-off. Figure 3.5 represents the results in which the Marangoni terms are turned off but we see the similar behavior of retardation as in Figure 3.4.

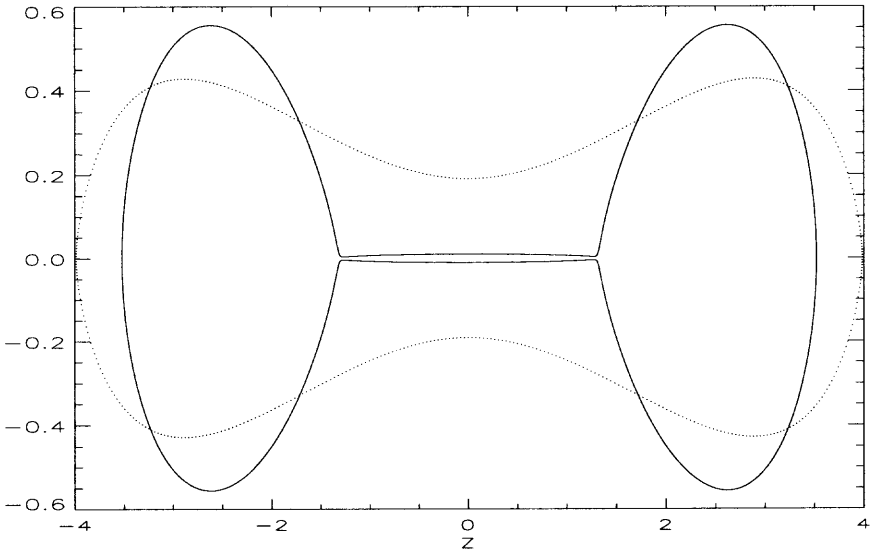

Figure 3.4 Results for the inviscid jet with full numerical simulations.

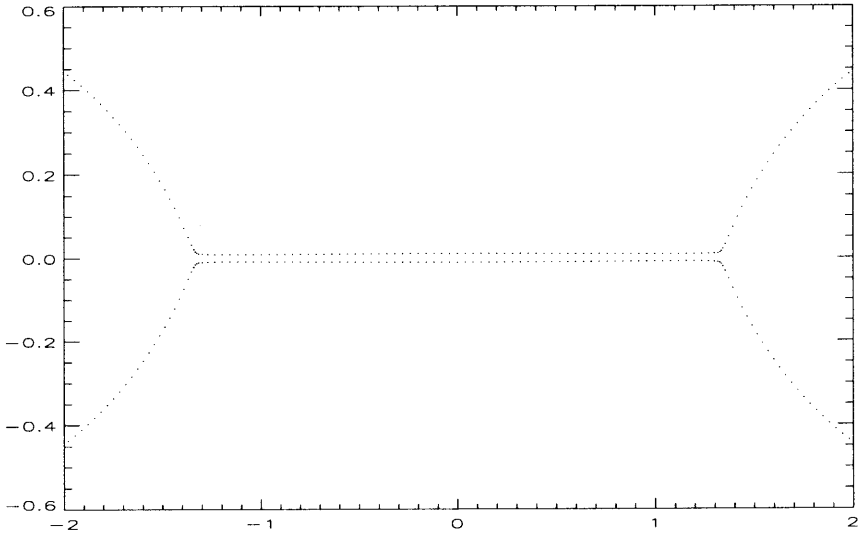

Figure 3.5 Results for the inviscid jet with full numerical with no Marangoni terms.

3.7 Effect of Surface Diffusion

In surface tension driven flows, Marangoni stresses develop due to the non-uniform distribution of surfactant. These are surface tension gradients which act in a way to make the surfactant concentration more uniform. In our asymptotic analysis, Marangoni terms do not appear in our final equations and boundary conditions. The reason is that the tangential stress balance (which incorporates the Marangoni force terms) decouples from the other equations and hence does not influence the long wave dynamics at the leading order. As a simple way of incorporating the Marangoni terms into the leading order equations, we tried rescaling the various parameters and dependant variables, with a hope that a particular scaling would re-couple the tangential stress balance and Stokeslet density $f(z,t)$ to the leading order equations. This would have the effect of re-introducing the Marangoni force terms to the leading order equations. Unfortunately, as shown in Appendix A, it is not possible to implement this re-coupling in consistent asymptotic expansion via a simple rescaling of parameters or variables.

In order to include a redistribution mechanism for surfactant, we next consider the effect of surface diffusion of surfactant concentration, characterized by the Peclet number $Pe_s = \frac{\sigma_o L}{D_s \mu}$. Surface diffusion is usually small and the effect is neglected in most cases. In present situation, the long wave model (3.50) and (3.51) does not predict pinch-off. If we run simulations for longer time, a shock develops and the model breaks down without predicting pinch-off. But as the slope steepens, surface diffusion effects become important due to large interfacial gradients.

When surface diffusion is incorporated into the model, the leading order asymptotic equations for surfactant transport (with diffusion) and for the jet radius are given by

$$\frac{\partial \Gamma}{\partial t} = -\frac{\Gamma}{2R}[Rp_i + \beta\Gamma - 1] + \frac{1}{Pe_o}[\Gamma_{zz} + \frac{R'\Gamma'}{R}], \tag{3.55}$$

$$\frac{\partial R}{\partial t} = \frac{1}{2}(Rp_i + \beta\Gamma - 1). \tag{3.56}$$

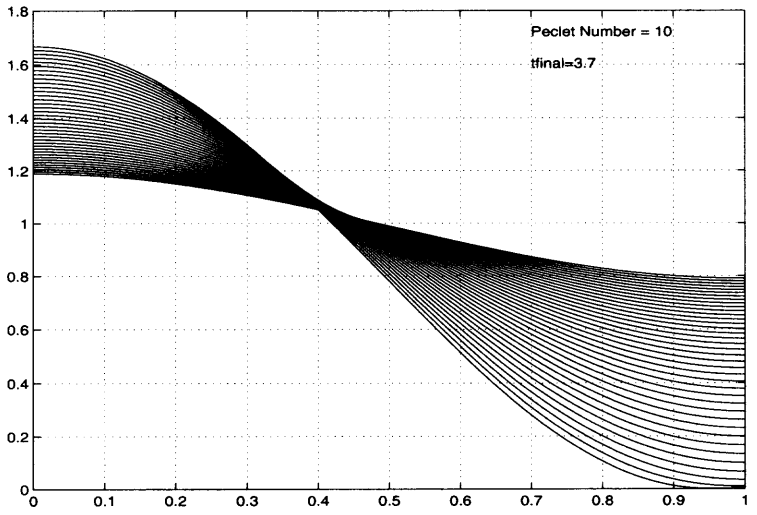

Figure 3.6 Jet radius at Peclet number=10.

The inside pressure is

$$p_i = \frac{1}{2}\int_{-1}^{1} \sigma R dz. \tag{3.57}$$

And

$$Pe_o = \frac{Pe_s}{\epsilon}. \tag{3.58}$$

To solve the above system, we first evaluate the integral using a trapezoidal rule to get the inside pressure. When the inside pressure is known, we use an implicit scheme, i.e., we use forward time and central space to discritize time and space derivatives. This discretization leads to a tridiagonal system of algebraic equations, which we solve using the Thomas algorithm.

Results of our numerical simulations for different values of Peclet number Pe_o are presented in this section. It is observed that for small values of the Peclet number, the jet pinches very fast (see Figure 3.6). As we increase the Peclet number, it takes longer for the jet to pinch. For high values of the Peclet number ($Pe_o = 1000$), a filament is formed (see Figure 3.9), as was seen in the case of infinite Peclet number (zero diffusion), but if we run simulations for longer time and as large gradients develop, surface diffusion effects become dominant and eventually cause the jet to pinch.

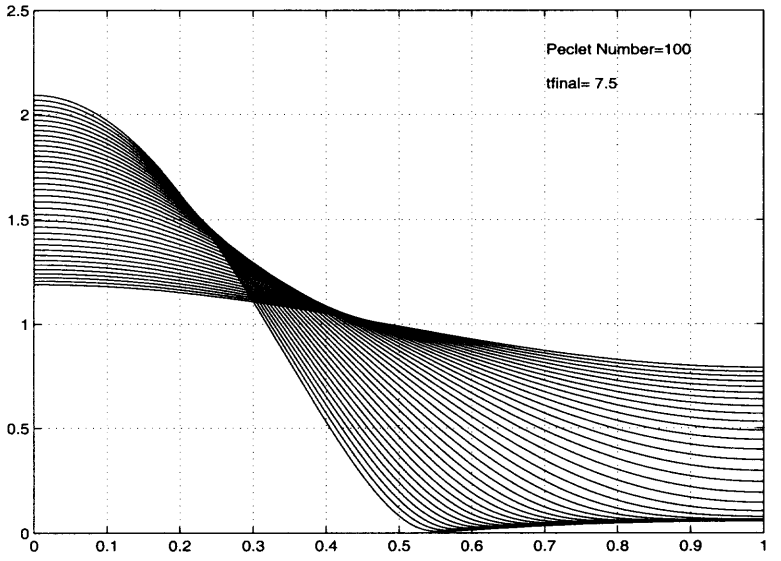

Figure 3.7 Jet radius at Peclet number 100.

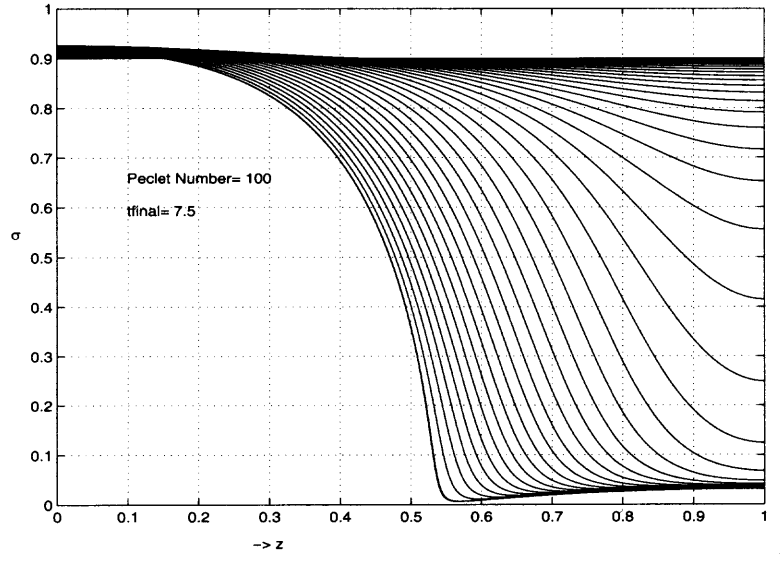

Figure 3.8 Surface tension at Peclet number=100.

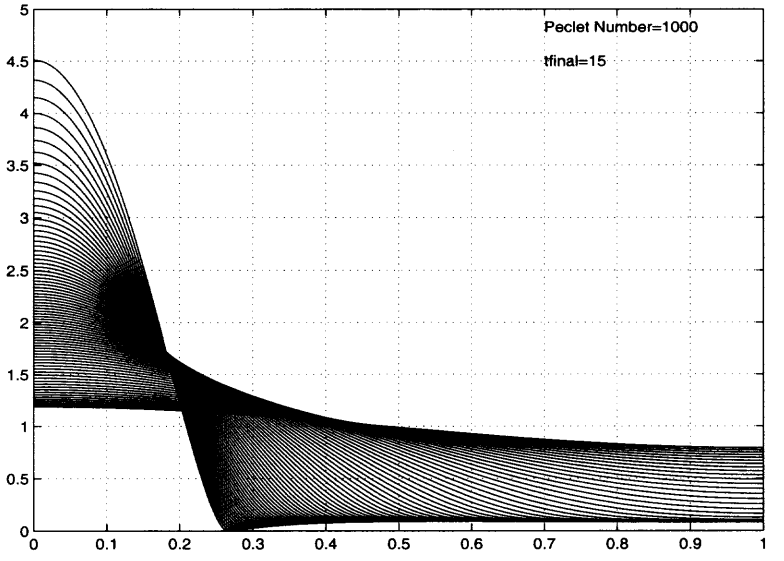

Figure 3.9 Jet radius at Peclet number=1000.

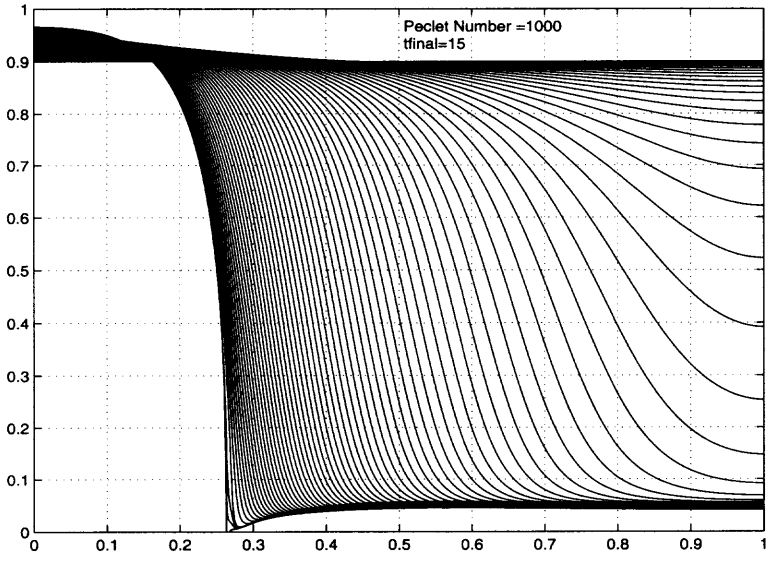

Figure 3.10 Surface tension at Peclet number=1000.

3.8 Results with Non-Linear Equation of State

The results described in the previous sections are obtained using a linear equation of state to express the relationship between surface tension and surfactant concentration, which is often appropriate for low or dilute surfactant concentration. In this section, we generalize our earlier analysis to include a non-linear equation of state. It is a more precise way of expressing this relationship and is appropriate for both high surfactant concentrations as well as for low concentrations.

Another motivation for using a non-linear equation of state is the fact that close to pinching, the surface area of the jet decreases, and as a result the amount of surfactant increases in the neck (filament). The assumption of dilute surfactant concentration is no longer true, and it is more appropriate to use a non-linear equation of state to express the relationship between the surface tension and the surfactant concentration. There are various forms of non-linear equations used in the literature [3]. The most frequently used also known as Langmuir equation [9] is given by

$$\sigma = \sigma_o[1 + \beta \ln(1 - \frac{\Gamma}{\Gamma_\infty})], \tag{3.59}$$

where σ_o represents the surface tension of the clean interface, Γ_∞ is the maximum concentration of surfactant and $\beta = \frac{RT\Gamma_\infty}{\sigma_o}$ is a dimensionless number with R as the universal gas constant and T as the absolute temperature. We non-dimensionalize the above the equation using the $\tilde{\sigma} = \frac{\sigma}{\sigma_o}$ and $\tilde{\Gamma} = \frac{\Gamma}{\Gamma_\infty}$, (and drop tildes) to get

$$\sigma = 1 + \beta \ln(1 - \Gamma). \tag{3.60}$$

Figure 3.11 and Figure 3.12 represent the results with the non-linear equation of state. Qualitatively, the results are similar to the ones with the linear equation of state and show that the presence of surfactant retards the pinch-off regardless of the equation of state used.

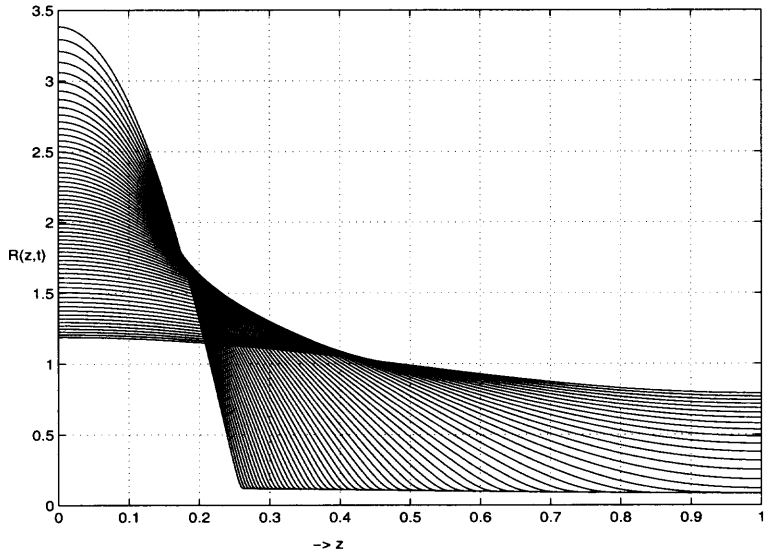

Figure 3.11 Jet radius with non-linear equation.

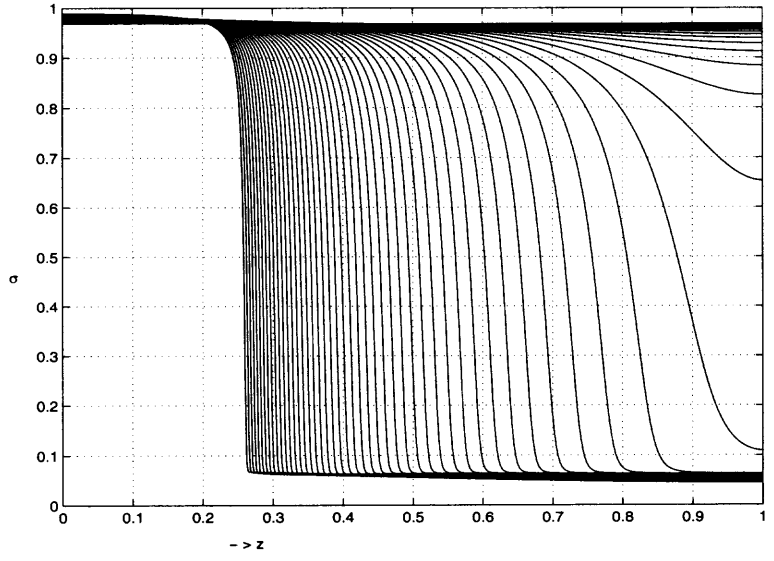

Figure 3.12 Surface tension with non-linear equation of state.

3.9 Diffusion and Non-linear Equation of State

In this section, we present the results with the combined effect of diffusion and non-linear equation of state. In this case governing equations become

$$\frac{\partial \Gamma}{\partial t} = -\frac{\Gamma}{2R}[Rp_i - \sigma(\Gamma)] - \frac{1}{Pe_o}[\frac{1}{R}\frac{\partial}{\partial z}(R\frac{\partial \Gamma}{\partial z})], \tag{3.61}$$

$$\frac{\partial R}{\partial t} = \frac{1}{2}[Rp_i - \sigma(\Gamma)], \tag{3.62}$$

where

$$\sigma(\Gamma) = 1 + \beta \ln(1 - \Gamma), \tag{3.63}$$

and Pe_o is the scaled surface Peclet number given by

$$Pe_o = \frac{Pe_s}{\epsilon}. \tag{3.64}$$

Inside the pressure is

$$p_i = \frac{1}{2}\int_{-1}^{1} \sigma R dz. \tag{3.65}$$

Figures 3.13 and 3.14 represents the results for the jet radius and surface tension given at different time steps during the evolution of the jet. Figure 3.13 shows the jet interface and we see the retardation effect even with the non-linear equation of state which results in the formation of a thin and long filament.

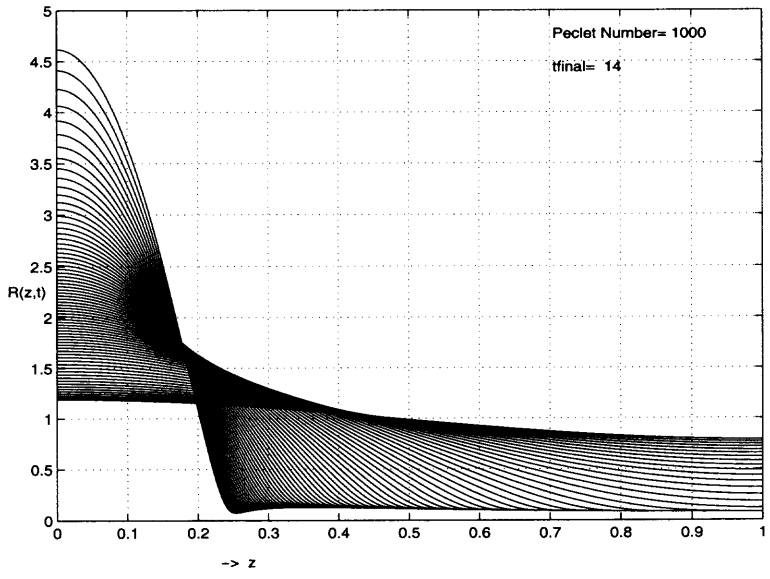

Figure 3.13 Jet radius R with non-linear equation of state and diffusion.

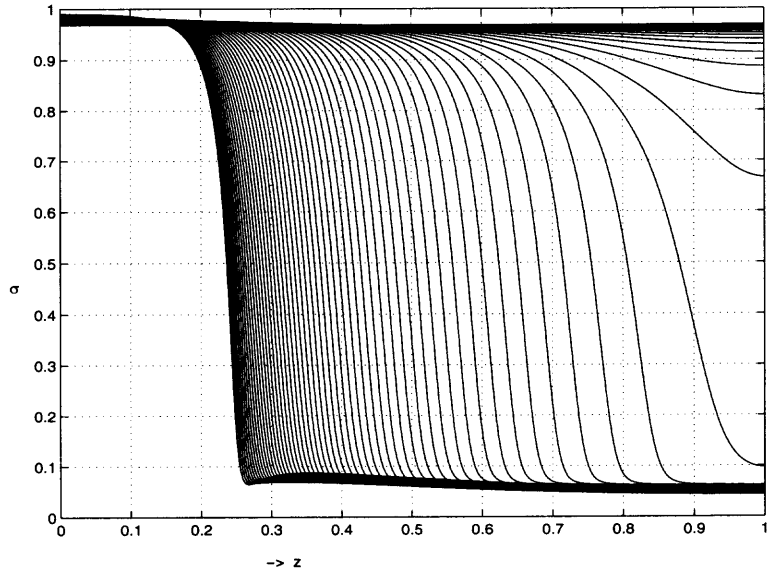

Figure 3.14 Surface tension σ with non-linear equation of state and diffusion.

3.10 Linear Stability Studies

3.10.1 Linear Stability of the Long Wave Model

We perform linear stability analysis of the governing equations obtained by using the approximations of the long wave theory. This will then be checked against the linear stability results of the full problem [14] in the long wave limit $k \to 0$, which is the region of validity of the long wave equations. Recall that governing equations are

$$\frac{\partial \Gamma}{\partial t} = -\frac{\Gamma}{2R}[Rp_i + \beta\Gamma - 1], \tag{3.66}$$

$$\frac{\partial R}{\partial t} = \frac{1}{2}[Rp_i + \beta\Gamma - 1], \tag{3.67}$$

and the inside pressure is given by the following integral

$$p_i = \frac{1}{2}\int_{-1}^{1} \sigma R dz. \tag{3.68}$$

We linearize R and Γ and p_i about the base states as follows

$$R = 1 + \delta\hat{R}cosk\pi z, \tag{3.69}$$

$$\Gamma = 1 + \delta\hat{\Gamma}cosk\pi z, \tag{3.70}$$

$$p_i = 1 - \beta, \tag{3.71}$$

where $\delta \ll 1$. Here, note that there is no correction to the pressure to the linear order. This can be proved by the conservation of volume condition. Substituting the above in the governing equations and collecting the terms to the order of δ we get

$$\hat{R}_t = \frac{(1-\beta)}{2}\hat{R} + \frac{\beta}{2}\hat{\Gamma}, \tag{3.72}$$

$$\hat{\Gamma}_t = \frac{(\beta-1)}{2}\hat{R} - \frac{\beta}{2}\hat{\Gamma}. \tag{3.73}$$

The above system of the ordinary differential equations can be written in the form

$$\mathbf{X}_t = A\mathbf{X},$$

where

$$\mathbf{X} = [\hat{R} \quad \hat{\Gamma}]^T, \tag{3.74}$$

and the matrix A is given by

$$A = \begin{bmatrix} \frac{(1-\beta)}{2} & \frac{\beta}{2} \\ \frac{(\beta-1)}{2} & -\frac{\beta}{2} \end{bmatrix}. \tag{3.75}$$

Stability of the system can be determined by finding the eigenvalues of the matrix A, which actually gives us the growth rate parameter s, where $[\hat{R}, \hat{\Gamma}] = e^{st}[\hat{R}_o, \hat{\Gamma}_o]$ with $\hat{R}_o$, $\hat{\Gamma}_o$ constants

$$s = \frac{1-2\beta}{2}, \qquad s = 0. \tag{3.76}$$

We note that when $\beta = 0$ (no surfactant case), this result is in agreement with the clean interface linear stability calculations of Tomotika [36] for $\mu_2 = 0$ and $k \to 0$, i.e., in the long wave limit.

A thorough linear stability analysis for the case of two fluid jet in the presence of soluble surfactant has been given by Hansen et al. [14]. In the next section, we verify that their expression (5.3), in zero surfactant solubility and $k \to 0$ limit, gives results that are in agreement with (3.76).

3.10.2 Comparison with Hansen's Results

Hansen et al. [14] investigated the effect of soluble surfactant on the breakup of a viscous filament surrounded by another viscous fluid using linear stability analysis. They studied the response of a fluid filament to small disturbances to the interface represented in terms of Fourier components. In the Stokes flow limit, they derived a dispersion relation for the case of a viscous thread in a viscous surrounding in the presence of a soluble surfactant.

To compare the linear stability results of long wave equations with the linear stability analysis of the Hansen [14], we start with the dispersion relation (5.3) in Hansen.

$$\omega_s\Big[\frac{1}{N_\mu}(1-\frac{1}{N_\mu})[G^2(k)-1-k^2]kF'(k)+(1-\frac{1}{N_\mu})[F^2(k)-1-k^2]kG'(k) +\frac{1}{N_\mu}[G(k)+F(k)]^2+(\frac{E_o}{\sigma_o})\frac{\kappa_s(\omega_s,k)}{2}(1+k^2)[kG'(k)+\frac{1}{N_\mu}kF'(k)]\Big] =\frac{1-k^2}{2}\Big[kG'(k)+\frac{1}{N_\mu}kF'(k)+(\frac{E_o}{\sigma_o})\frac{\kappa_s(\omega_s,k)}{2}kG'(k)kF'(k)\Big], \quad (3.77)$$

where

$$\kappa(\omega_s,k)=[\omega_s+\frac{k^2}{N_{sur}N_\sigma}+\frac{N_L}{N_{sc}N_\sigma}(k^2+N_{sc}N_\sigma\omega_s)^{1/2}]^{-1}, \quad (3.78)$$

$$kF'(k)=k^2-F^2(k)+2F(k), \quad (3.79)$$

$$kG'(k)=-k^2+G^2(k)+2G(k), \quad (3.80)$$

where ω_s is non-dimensional growth rate of the disturbances in the Stokes flow limit, $N_\sigma=\frac{\rho\sigma_o B}{\mu_i^2}$ is the surface tension number, $N_{sur}=\frac{\mu_i}{\rho D_s}$ is the surface diffusion number, $N_{sc}=\frac{\mu_i}{\rho D_\gamma}$ is the Schmidt number, $N_\mu=\frac{\mu_i}{\mu_o}$ is the viscosity ratio and $N_L=\frac{B}{K}$ is the interface thickness parameter. Here B denotes the undisturbed radius of the filament and K is the ratio of the interfacial concentration to the bulk concentration at

equilibrium. Also, $F(k) = \frac{kI_o(k)}{I_1(k)}$, $G(k) = \frac{kK_o(k)}{K_1(k)}$, where $I_\nu(k)$ and $K_\nu(k)$ are modified bessel functions of order ν.

To compare with the long wave model, we need to redefine the growth rate factor. Since ω_s is non-dimensionalized by $\frac{\sigma_o}{B\mu_i}$ and we are considering the case of an inviscid jet ($\mu_i \to 0$). Therefore, we define $\omega_H = \frac{\omega_s}{N_\mu}$, take $N_L = 0$, and $N_{sur} \to \infty$

$$\begin{aligned}\omega_H\Bigg[(1-\frac{1}{N_\mu})[G^2(k)-1-k^2]kF'(k)+(N_\mu-1)[F^2(k)-1-k^2]kG'(k)\\ +[G(k)+F(k)]^2+(\frac{E_o}{2\sigma_o})\frac{1}{\omega_H}(1+k^2)[kG'(k)+\frac{1}{N_\mu}kF'(k)]\Bigg]\\ =\frac{1-k^2}{2}\Bigg[kG'(k)+\frac{1}{N_\mu}kF'(k)+(\frac{E_o}{\sigma_o})\frac{1}{2N_\mu\omega_H}kG'(k)kF'(k)\Bigg].\end{aligned} \tag{3.81}$$

Multiplying (3.82) with N_μ on both sides and taking the limit as $N_\mu \to 0$, results in a dispersion relation for the case of an inviscid jet in viscous surrounding with insoluble surfactant

$$\begin{aligned}\omega_H\Bigg[kF'(k)[1+k^2-G^2(k)]+(\frac{E_o}{2\sigma_o})\frac{(1+k^2)}{\omega_H}kF'(k)]\Bigg]\\ =\frac{1-k^2}{2}\Bigg[kF'(k)+(\frac{E_o}{2\sigma_o})\frac{1}{\omega_H}kG'(k)kF'(k)\Bigg].\end{aligned} \tag{3.82}$$

Divide both sides by $kF'(k)$ and rearrange to get a quadratic equation for the growth rate ω_H

$$\begin{aligned}\omega_H^2\Big(1+k^2-G^2\Big)+\omega_H\Big(\frac{E_o(1+k^2)}{2\sigma_o}+\frac{(k^2-1)}{2}\Big)\\ +\frac{1}{4\sigma_o}\Big(E_o(k^2-1)(G^2-k^2+2G)\Big)=0,\end{aligned} \tag{3.83}$$

which is solved to give

$$\omega_H = \frac{-B \pm \sqrt{B^2-4AC}}{2A}, \tag{3.84}$$

where

$$A = 4k^2K_0^2 - 4K_1^2 - 4k^2K_1^2,$$

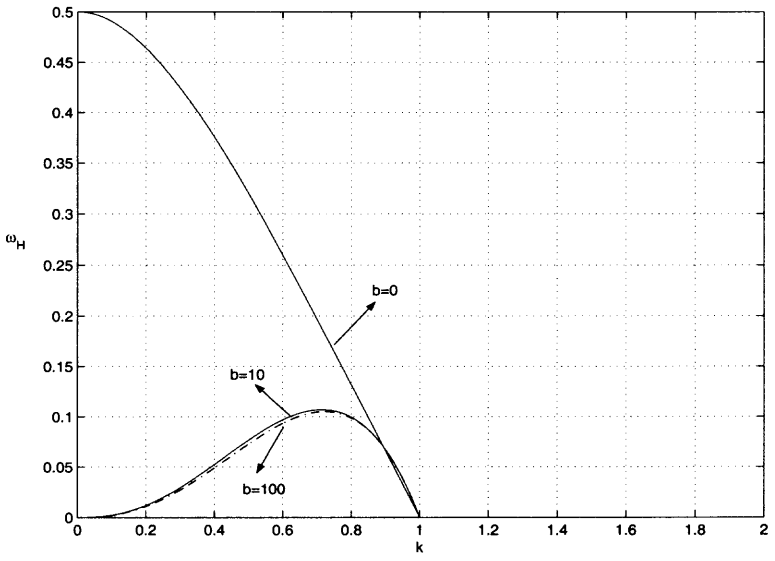

Figure 3.15 Growth rate ω_H for different values of $b = \frac{E_o}{\sigma_o}$.

$$B = 2K_1^2 - 2k^2K_1^2 - 2\frac{E_o}{\sigma_o}K_1^2,$$

$$C = \frac{E_o}{\sigma_o}k^3K_0^2 - \frac{E_o}{\sigma_o}k^5K_0^2 + 2k^2\frac{E_o}{\sigma_o}K_0K_1 - 2\frac{E_o}{\sigma_o}k^4K_0K_1 - \frac{E_o}{\sigma_o}k^3K_1^2 + k^5\frac{E_o}{\sigma_o}K_1^2.$$

Figure 3.15 represents the growth rate for ω_H plotted for different values of $b = \frac{E_o}{\sigma_o}$. It shows that there is small band of long wavelength unstable modes. Note that as $b \to \infty$, the dispersion approaches a limiting curve, where this is a growth for long waves with $k \to 0$, and the growth of all other waves is greatly reduced.

To compare with the long wave model, we take the limit($k \to 0$) of (3.84) and get the following growth rates for the two roots in (3.84):

$$\omega_H = \frac{\sigma_o - E_o}{2\sigma_o}, \quad \text{and} \quad \omega_H = 0. \tag{3.85}$$

Equation (3.85) shows the growth rates from the Hansen's results obtained in the long wavelength limit. This relation is given in the form of σ_o and E_o, surface tension and Gibbs elasticity for the undisturbed jet. To compare with our results, we express (3.85) in terms of β, and find (see Appendix B)

$$\frac{E_o}{\sigma_o} = \frac{\beta}{1-\beta}. \tag{3.86}$$

Using (3.86) in (3.85) yeilds

$$\omega_H = \frac{1-2\beta}{2(1-\beta)}, \quad \text{and} \quad \omega_H = 0. \tag{3.87}$$

The growth rates in (3.87) can be shown to be identical to the growth rates obtained from the long wave equations (see 3.76). The extra factor $(1-\beta)$ in the denominator is due to the different non-dimensionalization of time in both studies. For further details please see Appendix B.

3.10.3 Linear Stability of Long Wave Model with Diffusion

In this section, we present linear stability analysis of the long wave equations including the effect of diffusion. This will then be compared with the linear stability results of the full problem in the limit $k \to 0$ in Hansen et al. [14]. Recall the governing equations

$$\frac{\partial \Gamma}{\partial t} = -\frac{\Gamma}{2R}[Rp_i + \beta\Gamma - 1] + \frac{1}{Pe_o}[\Gamma_{zz} + \frac{R'\Gamma'}{R}], \tag{3.88}$$

$$\frac{\partial R}{\partial t} = \frac{1}{2}[Rp_i + \beta\Gamma - 1]. \tag{3.89}$$

We linearize R and Γ and p_i about the base states as follows

$$R = 1 + \delta\hat{R}cosk\pi z, \tag{3.90}$$

$$\Gamma = 1 + \delta\hat{\Gamma}cosk\pi z, \tag{3.91}$$

$$p_i = 1 - \beta, \tag{3.92}$$

where $\delta \ll 1$. Substituting in the governing equations and collecting the terms to the order of δ we get

$$\hat{R}_t = \frac{(1-\beta)}{2}\hat{R} + \frac{\beta}{2}\hat{\Gamma}, \tag{3.93}$$

$$\hat{\Gamma}_t = \frac{(\beta-1)}{2}\hat{R} - (\frac{\beta}{2} + \frac{k^2\pi^2}{Pe_o})\hat{\Gamma}. \tag{3.94}$$

The above system of the ordinary differential equations can be written in the form

$$\mathbf{X}_t = A\mathbf{X},$$

where

$$\mathbf{X} = [\hat{R} \quad \hat{\Gamma}]^T, \tag{3.95}$$

and the matrix A is given by

$$A = \begin{bmatrix} \frac{(1-\beta)}{2} & \frac{\beta}{2} \\ \frac{(\beta-1)}{2} & -\frac{\beta}{2} - \frac{k^2\pi^2}{Pe_o} \end{bmatrix}. \tag{3.96}$$

Stability of the system can be determined by finding the eigenvalues of the matrix A, which actually gives us the growth rate parameter s, where $[\hat{R}, \hat{\Gamma}] = e^{st}[\hat{R}_o, \hat{\Gamma}_o]$ with $\hat{R}_o$, $\hat{\Gamma}_o$ constants,

$$s = \frac{Pe_o - 2k^2\pi^2 - 2Pe_o\beta \pm \sqrt{{Pe_o}^2 + 4k^2Pe_o + 4k^4\pi^4 - 4{Pe_o}^2\beta + 4{Pe_o}^2\beta^2}}{4Pe_o}. \tag{3.97}$$

In the $k \to 0$ limit, we get

$$s = \frac{Pe_o - 2Pe_o\beta \pm \sqrt{(Pe_o - 2Pe_o\beta)^2}}{4Pe_o}. \tag{3.98}$$

Further simplification gives the growth rates as

$$s = \frac{1-2\beta}{2}, \quad s = 0. \tag{3.99}$$

3.10.4 Linear Stability of the Full Problem with Diffusion (Hansen)

The linear stability analysis of the the full problem with diffusion was considered by Hansen et al. [14]. We start with the dispersion relation (5.3) in Hansen.

$$\omega_s\Bigg[\frac{1}{N_\mu}(1-\frac{1}{N_\mu})[G^2(k)-1-k^2]kF'(k)+(1-\frac{1}{N_\mu})[F^2(k)-1-k^2]kG'(k)$$
$$+\frac{1}{N_\mu}[G(k)+F(k)]^2+(\frac{E_o}{\sigma_o})\frac{\kappa_s(\omega_s,k)}{2}(1+k^2)[kG'(k)+\frac{1}{N_\mu}kF'(k)]\Bigg]$$
$$=\frac{1-k^2}{2}\Bigg[kG'(k)+\frac{1}{N_\mu}kF'(k)+(\frac{E_o}{\sigma_o})\frac{\kappa_s(\omega_s,k)}{2}kG'(k)kF'(k)\Bigg], \quad (3.100)$$

where

$$\kappa(\omega_s,k)=\left[\omega_s+\frac{k^2}{N_{sur}N_\sigma}+\frac{N_L}{N_{sc}N_\sigma}(k^2+N_{sc}N_\sigma\omega_s)^{1/2}\right]^{-1}, \quad (3.101)$$

$$kF'(k)=k^2-F^2(k)+2F(k), \quad (3.102)$$

$$kG'(k)=-k^2+G^2(k)+2G(k). \quad (3.103)$$

We define a new growth rate factor by $\omega_H=\frac{\omega_s}{N_\mu}$ and take $N_L=0$. In this analysis, the parameter $N_{sur}=\frac{\mu_i}{\rho D_s}$ is retained due to the presence of surface diffusion.

$$\kappa(\omega_s,k)=\left(\omega_s+\frac{k^2}{N_{sur}N_\sigma}\right)^{-1}. \quad (3.104)$$

Use $\omega_H=\frac{\omega_s}{N_\mu}$ to get

$$\kappa(\omega_H,k)=\frac{Pe_o}{N_\mu(Pe_o\omega_H+k^2)}. \quad (3.105)$$

Note that

$$Pe_o\equiv N_\sigma N_{sur}N_\mu=\frac{\sigma_o B}{\mu D_s}, \quad (3.106)$$

is the Peclet number based on the jet width B

$$\omega_H\Big[(1-\frac{1}{N_\mu})[G^2(k)-1-k^2]kF'(k)+(N_\mu-1)[F^2(k)-1-k^2]kG'(k) \\ +[G(k)+F(k)]^2+(\frac{E_o}{2\sigma_o})\frac{Pe_o(1+k^2)}{(Pe_o\omega_H+k^2)}[kG'(k)+\frac{1}{N_\mu}kF'(k)]\Big] \\ =\frac{1-k^2}{2}\Big[kG'(k)+\frac{1}{N_\mu}kF'(k)+(\frac{E_o}{2\sigma_o})\frac{kG'(k)kF'(k)}{N_\mu(Pe_o\omega_H+k^2)}\Big]. \quad (3.107)$$

Multiplying with N_μ on both sides and taking limit as $N_\mu \to 0$, we get a dispersion relation for the case of an inviscid jet with insoluble surfactant with the effect of surface diffusion

$$\omega_H\Big[kF'(k)[1+k^2-G^2(k)]+\frac{E_oPe_o(1+k^2)kF'(k)}{2\sigma_o(Pe_o\omega_H+k^2)}\Big] \\ =\frac{1-k^2}{2}\Big[kF'(k)+\frac{E_oPe_okG'(k)kF'(k)}{2\sigma_o(Pe_o\omega_H+k^2)}\Big]. \quad (3.108)$$

Divide both sides by $kF'(k)$ to get

$$\omega_H\Big[(1+k^2-G^2(k))+\frac{E_oPe_o(1+k^2)}{2\sigma_o(Pe_o\omega_H+k^2)}\Big]=\frac{1-k^2}{2}\Big[1+\frac{E_oPe_okG'(k)}{2\sigma_o(Pe_o\omega_H+k^2)}\Big] \quad (3.109)$$

We use mathematica to find the roots of the above equation

$$\omega_H=\frac{-B\pm\sqrt{B^2-4AC}}{2A}, \quad (3.110)$$

where

$$A=-4k^2Pe_sK_0^2+4Pe_sK_1^2+4k^2Pe_sK_1^2,$$

$$B=-4k^4K_0^2+4k^2K_1^2+4k^4K_1^2-2Pe_sK_1^2+2k^2Pe_sK_1^2+ \\ 2Pe_s\frac{E_o}{\sigma_o}k^2K_1^2+2k^2Pe_s\frac{E_o}{\sigma_o}K_1^2,$$

$$C=-k^2Pe_s\frac{E_o}{\sigma_o}K_o^2+k^4Pe_s\frac{E_o}{\sigma_o}K_o^2-2kPe_s\frac{E_o}{\sigma_o}K_oK_1+2k^3Pe_s\frac{E_o}{\sigma_o}K_oK_1-2k^2K_1^2+ \\ 2k^4K_1^2+k^2Pe_s\frac{E_o}{\sigma_o}K_1^2-k^4Pe_s\frac{E_o}{\sigma_o}K_1^2.$$

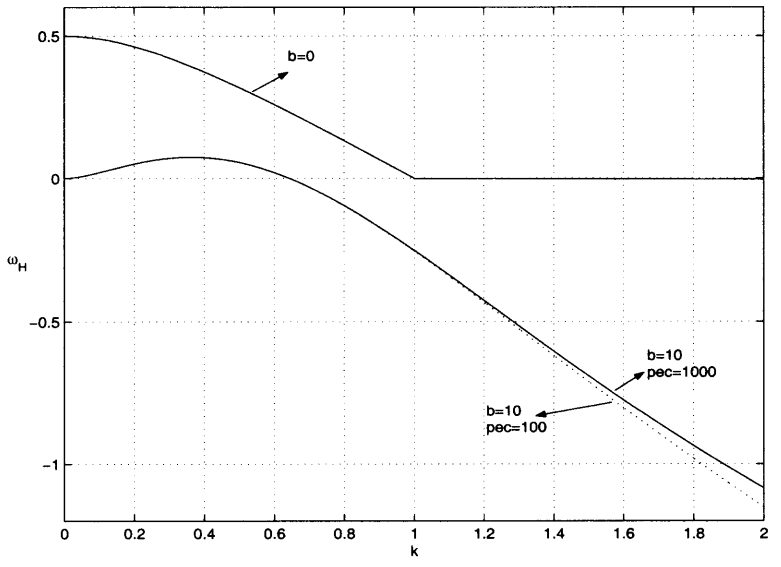

Figure 3.16 Growth rate vs wave number with diffusion.

Figure 3.16 shows the results of the linear stability analysis of the full problem with surface diffusion. Growth rate is plotted against the wave number for different values of the Peclet number and $\frac{E_o}{\sigma_o}$.

We take the long wavelength limit($k \rightarrow 0$) of (3.110) and get the following growth rates

$$\omega_H = \frac{\sigma_o - E_o}{2\sigma_o}, \quad \text{and} \quad \omega_H = 0. \tag{3.111}$$

After substituting

$$\frac{E_o}{\sigma_o} = \frac{\beta}{1-\beta}, \tag{3.112}$$

we get

$$\omega_H = \frac{1-2\beta}{2(1-\beta)}, \quad \text{and} \quad \omega_H = 0, \tag{3.113}$$

which are the same as growth rates obtained from the long wave equations (see 3.76); the extra factor $(1-\beta)$ in the denominator is due to the different non-dimensionalization of time in both studies. For further details please see Appendix B. Not surprisingly, the $k \rightarrow 0$ limit of the dispersion relation does not exhibit any dependance on the Peclet number, since diffusion is a high k effect.

CHAPTER 4

BREAKUP OF VISCOUS JET IN VISCOUS SURROUNDING IN PRESENCE OF INSOLUBLE SURFACTANT

In this Chapter, we generalize our earlier model of inviscid jet to consider the case of a slightly viscous jet in viscous surrounding. The case of inviscid jet becomes a special case of this study. We consider a less viscous fluid inside the jet and highly viscous fluid outside the jet. Both the jet and the external fluid are assumed to be incompressible, immiscible and Newtonian.

4.1 Derivation of the Model

We derive long wave evolution equations for a viscous fluid jet of viscosity μ_1(previously μ_1 was taken to be zero), surrounded by another viscous fluid of viscosity μ_2. Inside pressure of the jet is denoted by p_1, and outside pressure is p_2. Velocity vectors in a curvilinear polar coordinate system are denoted by (u_z, u_r, u_θ) for the inner fluid and (U_z, U_r, U_θ) for the outer fluid. We assume that both inner and outer fluids are described by Stokes equations for viscous flow. The inside flow is governed by the axisymmetric Stokes equations and continuity equation. Introduce the following dimensionless variables

$$z' = \frac{z}{L}, \quad r' = \frac{r}{L}, \quad u' = \frac{\mu_2}{\sigma_o}u, \quad t' = \frac{\sigma_o}{\mu B}t,$$

$$\Gamma' = \frac{\Gamma}{\Gamma_o}, \; p_2' = \frac{L}{\sigma_o}p_2 \quad p_1' = \frac{B}{\sigma_o}p_1, \quad \epsilon = B/L.$$

The non-dimensionalization of interior pressure by the jet radius is motivated by the fact that instability is capillary driven. We introduce the viscosity ratio $\frac{\mu_1}{\mu_2} = \lambda$. For equations governing the flow of interior fluid, we introduce the new scaling $\tilde{r} = \frac{r}{\epsilon}$, using the slenderness of the jet.

With the new scalings, inside equations become

$$\frac{\lambda}{\epsilon}\left(\frac{1}{\tilde{r}}\frac{\partial}{\partial\tilde{r}}(\tilde{r}\frac{\partial u_z}{\partial\tilde{r}})+\epsilon^2\frac{\partial^2 u_z}{\partial z^2}\right)=\frac{\partial p_1}{\partial z}. \tag{4.1}$$

$$\lambda\left(\frac{1}{\tilde{r}}\frac{\partial}{\partial\tilde{r}}(\tilde{r}\frac{\partial u_r}{\partial\tilde{r}})-\frac{u_r}{\tilde{r}^2}+\epsilon^2\frac{\partial^2 u_r}{\partial z^2}\right)=\frac{\partial p_1}{\partial\tilde{r}}. \tag{4.2}$$

The continuity equation after scaling becomes

$$\epsilon\frac{\partial u_z}{\partial z}+\frac{1}{\tilde{r}}\frac{\partial}{\partial\tilde{r}}(\tilde{r}u_r)=0. \tag{4.3}$$

We also assume that $\frac{\partial p_1}{\partial z}=O(1)$, since the instability is capillary driven. Note that this implies $\frac{\lambda}{\epsilon}u_z=O(1)$ so that

$$u_z=O(\frac{\epsilon}{\lambda}), \tag{4.4}$$

and from (4.3)

$$u_r=O(\frac{\epsilon^2}{\lambda}). \tag{4.5}$$

Alternatively, $\frac{\lambda}{\epsilon}u_z\gg 1$, which gives a different scaling regime which we do not consider here.

The non-dimensional tangential stress balance (T.S.B) and normal stress balance (N.S.B) are given by

T.S.B:

$$\lambda\left[\tilde{R}'\frac{\partial u_r}{\partial\tilde{r}}+(1-\epsilon^2\tilde{R}'^2)\frac{1}{2}(\frac{\partial u_r}{\partial z}+\frac{1}{\epsilon}\frac{\partial u_z}{\partial\tilde{r}})-\epsilon\tilde{R}'\frac{\partial u_z}{\partial z}\right]-\epsilon\tilde{R}'\frac{\partial U_r}{\partial r}-(1-\epsilon^2\tilde{R}'^2)\frac{1}{2}(\frac{\partial U_r}{\partial z}+\frac{\partial U_z}{\partial r})$$
$$+\epsilon\tilde{R}'\frac{\partial U_z}{\partial z}=\frac{\partial\Gamma}{\partial z}\frac{\beta}{\sqrt{1+\epsilon^2\tilde{R}'^2}} \tag{4.6}$$

N.S.B:

$$p_1-\epsilon p_2-\frac{2\epsilon\lambda}{(1+\epsilon^2\tilde{R}'^2)}\left[\frac{1}{\epsilon}\frac{\partial u_r}{\partial\tilde{r}}-\epsilon\tilde{R}'(\frac{\partial u_r}{\partial z}+\frac{1}{\epsilon}\frac{\partial u_z}{\partial\tilde{r}})+\epsilon^2\tilde{R}'^2\frac{\partial u_z}{\partial z}\right]+\frac{2\epsilon}{(1+\epsilon^2\tilde{R}'^2)}\frac{\partial U_r}{\partial r}$$
$$-\frac{2\epsilon}{(1+\epsilon^2\tilde{R}'^2)}\left[\epsilon\tilde{R}'(\frac{\partial U_r}{\partial z}+\frac{\partial U_z}{\partial r})-\epsilon^2\tilde{R}'^2\frac{\partial U_z}{\partial z}\right]=\frac{\sigma(\Gamma)}{\tilde{R}\sqrt{1+\epsilon^2\tilde{R}'^2}}\left[1-\frac{\epsilon^2\tilde{R}\tilde{R}''}{1+\epsilon^2\tilde{R}'^2}\right] \tag{4.7}$$

where primes denote $\frac{\partial}{\partial z}$ and the quantities in the interior of the jet have been rescaled by $\tilde{r} = \frac{r}{\epsilon}$.

The non-dimensional surfactant transport equation is given by

$$\frac{\partial \Gamma}{\partial t} + \frac{\epsilon}{R\sqrt{1+\epsilon^2 R'^2}} \frac{\partial}{\partial z}\left[\frac{R\Gamma}{\sqrt{1+\epsilon^2 R'^2}}(\epsilon u_r R' + u_z)\right] - \frac{\epsilon^2 R'}{1+\epsilon^2 R'^2}\frac{\partial R}{\partial t}\frac{\partial \Gamma}{\partial z} \tag{4.8}$$
$$\frac{\epsilon}{Pe_s}\left[\frac{1}{R\sqrt{1+\epsilon^2 R'^2}}\frac{\partial}{\partial z}\left(\frac{R}{\sqrt{1+\epsilon^2 R'^2}}\frac{\partial \Gamma}{\partial z}\right)\right] + \frac{\Gamma(u_r - \epsilon R' u_z)}{R(1+\epsilon^2 R'^2)}\left[1 - \frac{\epsilon^2 R R''}{1+\epsilon^2 R'^2}\right] = 0,$$

where we have introduced a surface Peclet number $Pe_s = \frac{\sigma_o L}{D_s \mu}$.

The kinematic condition is

$$u_r = \frac{\partial R}{\partial t} + \epsilon u_z \frac{\partial R}{\partial z}. \tag{4.9}$$

4.2 Method of Solution

In the exterior of the jet (as in the case of inviscid jet), we can approximate the leading order solution of the Stokes equations in the form of integrals of Stokeslet and source terms over the jet centerline. Using the method of Handelsman and Keller [13], we can write the localized expressions on the jet surface at $r = \epsilon\tilde{R}$

$$U_r \sim -2\epsilon\tilde{R}f' \ln\frac{1}{\epsilon\tilde{R}} + \frac{2g}{\epsilon\tilde{R}}, \tag{4.10}$$

$$U_z \sim 4f \ln\frac{1}{\epsilon\tilde{R}} - 2g' \ln\frac{1}{\epsilon\tilde{R}}, \tag{4.11}$$

$$p_2 \sim -4f' \ln\frac{1}{\epsilon\tilde{R}}, \tag{4.12}$$

$$\frac{\partial U_r}{\partial r} \sim -2f' \ln\frac{1}{\epsilon\tilde{R}} - 2g\frac{1}{\epsilon^2\tilde{R}^2}, \tag{4.13}$$

$$\frac{\partial U_z}{\partial z} \sim 4f' \ln\frac{1}{\epsilon\tilde{R}} - 2g'' \ln\frac{1}{\epsilon\tilde{R}}, \tag{4.14}$$

$$\frac{\partial U_r}{\partial z} + \frac{\partial U_z}{\partial r} \sim 4g'\frac{1}{\epsilon\tilde{R}} - 4f\frac{1}{\epsilon\tilde{R}}, \tag{4.15}$$

where we have kept leading order terms in f and g. Note that scales for f and g are not known at this point and will be determined by matching with the inner solution.

4.3 Order of Magnitude Analysis

In this section, we perform an order-of-magnitude analysis of the equations and boundary conditions. First, consider the tangential stress balance; using (4.4), (4.5) and (4.13)-(4.15), we equate the leading order contribution on both sides of T.S.B to get

$$\frac{\lambda}{2}\frac{\partial u_z}{\partial \tilde{r}} + \frac{2\tilde{R}'g}{\epsilon\tilde{R}^2} + \frac{2f}{\epsilon\tilde{R}} - \frac{2g'}{\epsilon\tilde{R}} \sim \beta\frac{\partial \Gamma}{\partial z}. \tag{4.16}$$

Since $\lambda\frac{\partial u_z}{\partial \tilde{r}} \sim O(1)$ from (4.4), this suggests that

$$\frac{f}{\epsilon}, \frac{g}{\epsilon} = O(1). \tag{4.17}$$

Leading order terms in the normal stress balance yield

$$p_1 - 2\lambda\frac{\partial u_r}{\partial \tilde{r}} - 2\epsilon\frac{\partial U_r}{\partial r} = \frac{\sigma}{\tilde{R}}, \tag{4.18}$$

where $\frac{\partial U_r}{\partial r}$ is given by (4.13). We shall eventually find that the second term in the above equation is of a higher order.

Continuity of Velocity:

From the continuity of the axial component of the velocity we have,

$$u_z = U_z \quad \text{at the interface,} \tag{4.19}$$

where the value of U_z at the interface $r = \epsilon\tilde{R}$ is given by

$$U_z \sim 4f \ln\frac{1}{\epsilon} - 2g' \ln\frac{1}{\epsilon}. \tag{4.20}$$

From (4.4) and (4.20), order of magnitude analysis yields

$$u_z \sim \frac{\epsilon}{\lambda} \sim O\left(f \ln\frac{1}{\epsilon}, g \ln\frac{1}{\epsilon}\right) \tag{4.21}$$

From the continuity of the radial component of the velocity at the interface we have

$$u_r = U_r \quad \text{at} \quad r = \epsilon\tilde{R}. \tag{4.22}$$

Thus, (4.5), (4.10) and (4.22) imply that

$$u_r \sim \frac{\epsilon^2}{\lambda} \sim O\left(f'\epsilon \ln\frac{1}{\epsilon}, \frac{2g}{\epsilon}\right). \tag{4.23}$$

A consistent scaling for (4.17), (4.18), (4.21) and (4.23) is

$$\begin{aligned} f \sim g \sim \epsilon, \qquad & \lambda \sim \epsilon^2, \\ u_z \sim \frac{1}{\epsilon}, \qquad & u_r \sim 1. \end{aligned} \tag{4.24}$$

Remark:

The scalings for the viscosity ratio, i.e., $\lambda \sim O(\epsilon^2)$ give a distinguished balance. We could have no different scaling for f and g with $\lambda \sim O(\epsilon^2)$ which give a different distinguished balance. However there exits other scalings for λ satisfying $\lambda \gg 1$ (e.g., $\lambda \sim O(\frac{1}{\ln\epsilon})$, or $\lambda \sim O(\frac{1}{\lambda^2 \ln\epsilon})$) for which distinguished balance can be found. But in this study we are interested in small λ.

Motivated by these scalings, we let

$$\lambda = \epsilon^2\lambda_0, \quad f = \epsilon f_0, \quad g = \epsilon g_0, \quad u_z = \frac{\tilde{u}_z}{\epsilon}, \quad u_r \sim \tilde{u_r}, \tag{4.25}$$

$$f_0 = O(1), \quad g_0 = O(1), \quad \lambda_0 = O(1). \tag{4.26}$$

Using these new scalings in Stokes equations given by (4.1) and (4.2), we get

$$\lambda_0\left[\frac{1}{\tilde{r}}\frac{\partial}{\partial\tilde{r}}(\tilde{r}\frac{\partial\tilde{u}_z}{\partial\tilde{r}}) + \epsilon\frac{\partial^2\tilde{u}_z}{\partial z^2}\right] = \frac{\partial p_1}{\partial z}, \tag{4.27}$$

$$\epsilon^2\lambda_0\left[\frac{1}{\tilde{r}}\frac{\partial}{\partial\tilde{r}}(\tilde{r}\frac{\partial\tilde{u}_r}{\partial\tilde{r}}) - \frac{\tilde{u}_r}{\tilde{r}^2} + \epsilon^2\frac{\partial^2\tilde{u}_r}{\partial z^2}\right] = \frac{\partial p_1}{\partial\tilde{r}}. \tag{4.28}$$

Order of magnitude analysis of the axial equation(4.27) suggests that the second term on the left hand side is negligible as compared with the other terms in the equation., so we get

$$\lambda_0 \left[\frac{1}{\tilde{r}} \frac{\partial}{\partial \tilde{r}} (\tilde{r} \frac{\partial \tilde{u}_z}{\partial \tilde{r}}) \right] = \frac{\partial p_1}{\partial z}. \tag{4.29}$$

Similarly, order of magnitude analysis of the radial component suggests that whole left hand side is negligible, so that

$$\frac{\partial p_1}{\partial \tilde{r}} = 0. \tag{4.30}$$

Therefore,

$$p_1 = p_1(z, t). \tag{4.31}$$

Multiply equation (4.29) by $\tilde{r}$ and integrate with respect to $\tilde{r}$ (using (4.31)) to get

$$\lambda_0 \frac{\partial \tilde{u}_z}{\partial \tilde{r}} = \frac{\tilde{r}}{2} \frac{\partial p_1}{\partial z} + \frac{C(z,t)}{\tilde{r}}. \tag{4.32}$$

Integrating again with respect to $\tilde{r}$, we get

$$\lambda_0 \tilde{u}_z = \frac{\tilde{r}^2}{4} \frac{\partial p_1}{\partial z} + C(z,t) \ln \tilde{r} + B(z,t), \tag{4.33}$$

where B and C are the constants of integration and are functions of z and t only. Moreover $\tilde{r} = 0$ is in our domain and we require a finite velocity at $\tilde{r} = 0$, hence, we choose $C = 0$ yielding

$$\lambda_0 \tilde{u}_z = \frac{\tilde{r}^2}{4} \frac{\partial p_1}{\partial z} + B(z,t). \tag{4.34}$$

Using equation (4.34) in the equation of continuity (4.3), we obtain

$$\frac{\tilde{r}^2}{4} \frac{d^2 p_1}{dz^2} + B'(z,t) + \frac{\lambda_0}{\tilde{r}} \frac{\partial}{\partial \tilde{r}} (\tilde{r} \tilde{u}_r) = 0. \tag{4.35}$$

Multiply throughout by $\tilde{r}$ and integrate with respect to $\tilde{r}$ to get

$$\frac{\tilde{r}^4}{16}\frac{d^2p_1}{dz^2} + \frac{\tilde{r}^2}{2}B'(z,t) + \lambda_0\tilde{r}\tilde{u}_r = 0. \tag{4.36}$$

$$\lambda_0\tilde{r}\tilde{u}_r = -\frac{\tilde{r}^4}{16}\frac{d^2p_1}{dz^2} - \frac{\tilde{r}^2}{2}B'(z,t). \tag{4.37}$$

From (4.16), we have a leading order equation for tangential stress balance:

$$\frac{\lambda_0}{2}\frac{\partial\tilde{u}_z}{\partial\tilde{r}} = -\frac{2\tilde{R}'g}{\epsilon\tilde{R}^2} - \frac{2f}{\epsilon\tilde{R}} + \frac{2g'}{\epsilon\tilde{R}} + \beta\frac{\partial\Gamma}{\partial z}. \tag{4.38}$$

But again we have an expression for $\tilde{u}_z$ given by

$$\lambda_0\tilde{u}_z = \frac{\tilde{r}^2}{4}\frac{dp_1}{dz} + B(z,t).$$

Differentiating with respect to $\tilde{r}$ we get

$$\frac{\partial\tilde{u}_z}{\partial\tilde{r}} = \frac{1}{\lambda_0}\left(\frac{\tilde{r}}{2}\frac{dp_1}{dz}\right). \tag{4.39}$$

Substituting (4.39) in (4.38) and using $g = \epsilon g_0$ and $f = \epsilon f_0$, we get

$$\frac{\tilde{r}}{4}\frac{dp_1}{dz} = -\frac{2\tilde{R}'g_0}{\tilde{R}^2} - \frac{2f_0}{\tilde{R}} + \frac{2g_0'}{\tilde{R}} + \beta\frac{\partial\Gamma}{\partial z}. \tag{4.40}$$

Evaluating the above equation at $\tilde{r} = \tilde{R}$, we get

$$\frac{\tilde{R}}{4}\frac{dp_1}{dz} = -\frac{2\tilde{R}'g_0}{\tilde{R}^2} - \frac{2f_0}{\tilde{R}} + \frac{2g_0'}{\tilde{R}} + \beta\frac{\partial\Gamma}{\partial z}. \tag{4.41}$$

This equation determines the Stokeslet density f in terms of the source density g and the interface shape but otherwise decouples from the other leading order equations.

Consider next the normal stress balance (4.7). From the scalings (4.24) and using (4.10)-(4.15), we get the leading order contribution in the normal stress balance

$$p_1 + 2\epsilon\frac{\partial U_r}{\partial r} = \frac{\sigma}{\tilde{R}}. \tag{4.42}$$

Recall that

$$\frac{\partial U_r}{\partial r} \sim -2f' \ln \frac{1}{\epsilon} - \frac{2g}{\epsilon^2 \tilde{R}^2}. \tag{4.43}$$

Using (4.43) and (4.25) in (4.42), we get an expression for the leading order contribution in the normal stress balance:

$$p_1 - \frac{4g_0}{\tilde{R}^2} = \frac{\sigma}{\tilde{R}}. \tag{4.44}$$

Continuity of velocity:

Recall that continuity of velocity gives us

$$u_z = U_z \quad \text{at} \quad r = \epsilon \tilde{R}. \tag{4.45}$$

From (4.11), (4.25) and (4.34) we get

$$\frac{1}{\epsilon \lambda_0} \left[\frac{p_1' \tilde{R}^2}{4} + B \right] = O(\epsilon \ln \frac{1}{\epsilon}). \tag{4.46}$$

It follows that the left hand side of the above equation is zero to the leading order. The integration function B can be recovered from the above equation

$$B(z,t) = -\frac{p_1' \tilde{R}^2}{4}. \tag{4.47}$$

Inserting (4.47) into (4.37), radial component of velocity becomes

$$\tilde{u}_r = \frac{1}{\lambda_0} \left[\frac{\tilde{R}^3}{16} \frac{d^2 p_1}{dz^2} + \frac{p_1' \tilde{R}^2 \tilde{R}'}{4} \right]. \tag{4.48}$$

The leading order contribution from the normal stress balance is

$$p_1 - \frac{4g_0}{\tilde{R}^2} = \frac{\sigma}{\tilde{R}}. \tag{4.49}$$

Further simplification gives

$$\frac{p_1 \tilde{R} - \sigma}{2} = \frac{2g_0}{\tilde{R}}. \tag{4.50}$$

We know from the continuity of the radial component of velocity that

$$\tilde{u}_r = \frac{2g_0}{\tilde{R}}. \tag{4.51}$$

Comparing (4.50) and (4.51), we get

$$\tilde{u}_r = \frac{p_1\tilde{R} - \sigma}{2}. \tag{4.52}$$

To find the governing equation for the evolution of the interface, we use the leading order Kinematic condition given by

$$\tilde{u}_r = \tilde{R}_t. \tag{4.53}$$

From (4.52) and (4.53), we obtain an equation which governs the evolution of the interface:

$$\tilde{R}_t = \frac{p_1\tilde{R} - \sigma}{2}. \tag{4.54}$$

By comparing (4.48) with (4.52) we get a equation for the inside pressure

$$\frac{p_1\tilde{R} - \sigma}{2} = \frac{1}{\lambda_0}\left[\frac{\tilde{R}^3 p_1''}{16} + \frac{\tilde{R}^2\tilde{R}' p_1'}{4}\right], \tag{4.55}$$

i.e.,

$$p_1 - \frac{1}{\lambda_0}\left[\frac{\tilde{R}^2 p_1''}{8} + \frac{\tilde{R}\tilde{R}' p_1'}{2}\right] = \frac{\sigma}{\tilde{R}}, \tag{4.56}$$

where primes denote the derivative with respect to z and $\sigma = \sigma(\Gamma)$ is a variable surface tension, which can be a linear or non-linear function of surfactant concentration. Initially, we use a simple linear equation of state $\sigma = 1 - \beta\Gamma$, but other non-linear relationships can easily be incorporated into the model. Equation (4.56) is for the inside pressure. Recall that in the case of an inviscid jet, the inside pressure was spatially independent and was given in the form of an integral. But in this case, the inside pressure is governed by a boundary value problem given by this second order ordinary differential equation.

The evolution equation for the surfactant transport equation is obtained in the similar manner as in the inviscid case and is given by

$$\Gamma_t = -\frac{\Gamma}{2R}[p_1 R - \sigma]. \tag{4.57}$$

4.4 Numerical Solution

The complete set of equations governing the dynamics of a slightly viscous, axisymmetric and slender jet is given by (without tildes)

$$R_t = \frac{1}{2}[p_1 R - \sigma(\Gamma)], \tag{4.58}$$

$$\Gamma_t = -\frac{\Gamma}{2R}[p_1 R - \sigma(\Gamma)], \tag{4.59}$$

where the inside pressure p_1 is governed by the following second order differential equation.

$$p_1 - \frac{1}{\lambda_0}[\frac{R^2 p_1''}{8} + \frac{RR' p_1'}{2}] = \frac{\sigma}{R}. \tag{4.60}$$

In the absence of a surfactant, equations (4.58) and (4.60) have been obtained by Lister and Sierou [32] and Howell and Siegel [15]. Equations (4.58)-(4.60) are integrated using a finite difference method, which is explicit in time. We briefly describe the method. Assume the shape R is known at time t. The pressure is then determined from the boundary value problem (4.60)(with boundary conditions being 2π periodicity in z). We use central differences to discretize the equation; this leads to a tridiagonal matrix for the inside pressure, which is then easily solved using the Thomas algorithm. Once the pressure is known at time t, equations (4.58) and (4.59) are integrated using an explicit method to obtain R and Γ at time $t + \Delta t$.

Figures 4.1 and 4.2 show the jet radius plotted at various time steps. Figure 4.1 shows the radius without surfactant and we see that the trend suggests the jet

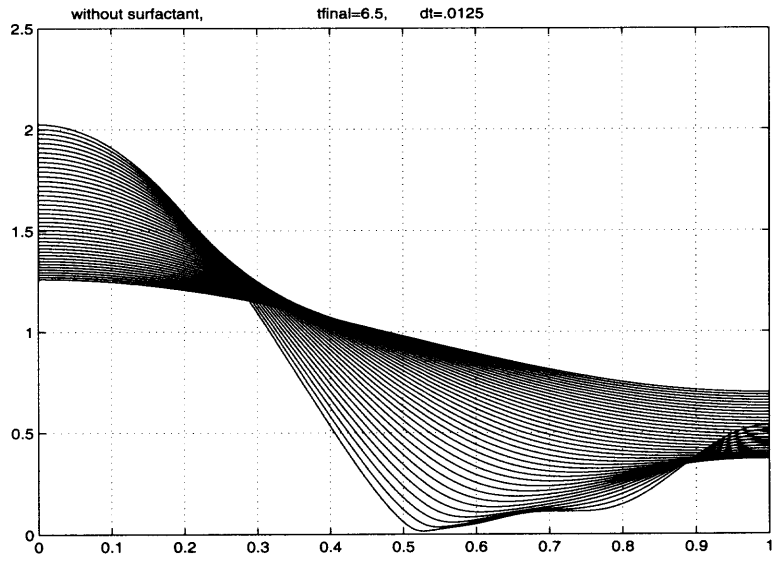

Figure 4.1 Jet radius $R(z,t)$ vs axial direction z, without surfactant.

pinch-off occurs in finite time. Similarity solutions to (4.58) and (4.59) (for $\sigma = 1$) which exhibits pinch-off in finite time have been found by Lister and Sierou [32].

On the other hand, Figure 4.2 shows the jet radius in presence of a surfactant, and we see that the presence of surfactant retards the pinch-off process. The finite time singularity, which is observed in the case of no surfactant, is inhibited in the formation of a thin and long filament.

4.5 Effect of Diffusion on Pinching

As was discussed earlier, due to the presence of large gradients of the surfactant concentration at the interface, surface diffusion of surfactant becomes important. We presently include the effect of surface diffusion into the model. In this section, we solve the governing equations including the effect of diffusion and present results for different values of the Peclet number.

The asymptotic equations governing the surfactant transport (with diffusion) and the jet radius are given by

$$\frac{\partial \Gamma}{\partial t} = -\frac{\Gamma}{2R}[Rp_i + \beta\Gamma - 1] + \frac{1}{Pe_o}\left[\frac{1}{R}\frac{\partial}{\partial z}(R\frac{\partial \Gamma}{\partial z})\right], \tag{4.61}$$

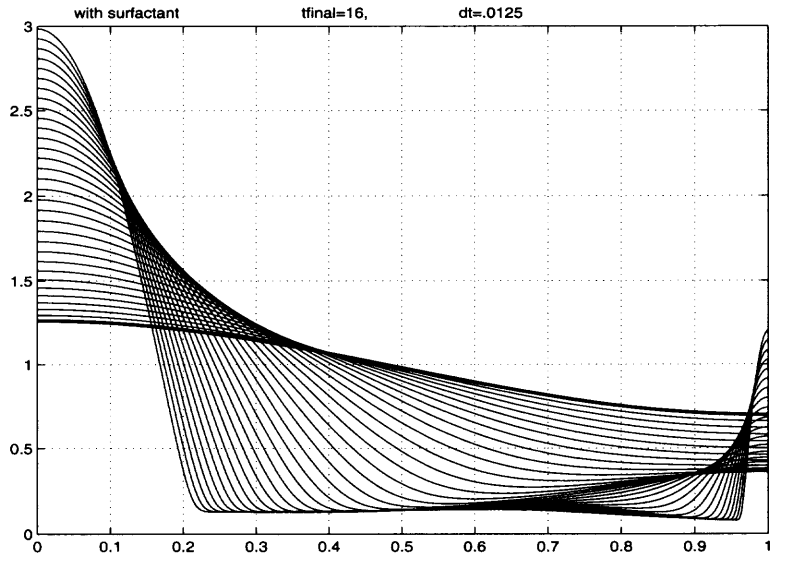

Figure 4.2 Jet radius $R(z,t)$ vs axial direction z, with surfactant.

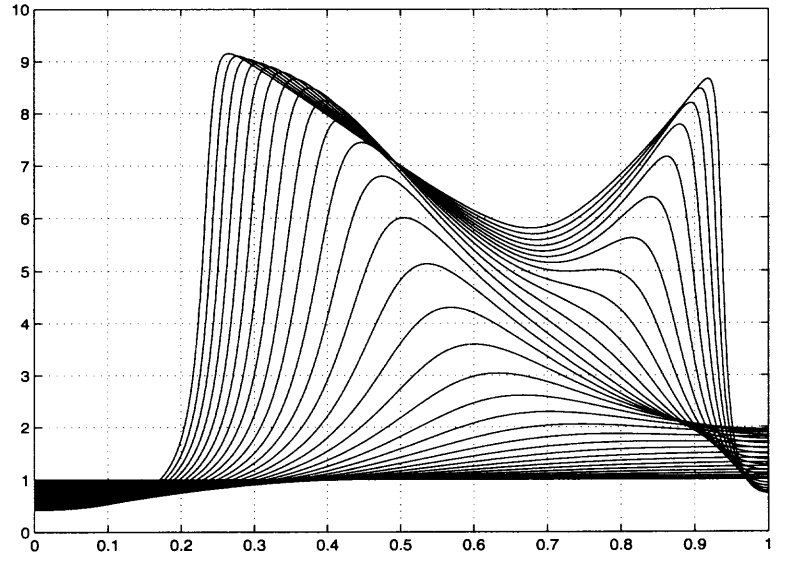

Figure 4.3 Surfactant concentration Γ vs axial direction z.

$$\frac{\partial R}{\partial t} = \frac{1}{2}(Rp_i + \beta\Gamma - 1). \tag{4.62}$$

The inside pressure p_1 is governed by the following second order differential equation.

$$p_1 - \frac{1}{\lambda_0}\left[\frac{R^2 p_1''}{8} + \frac{1}{2}RR'p_1'\right] = \frac{\sigma}{R}. \tag{4.63}$$

Here Pe_o is the scaled Peclet number

$$Pe_o = \frac{Pe_s}{\epsilon}.$$

Figures 4.4 - 4.6 show the results with the effects of diffusion. For high value of the Peclet number ($Pe_o = 1000$), a filament is formed (see Figure 4.4), as was seen in the case of infinite Peclet number (zero diffusion), but if we run the simulations for longer time and as large gradients develop, surface diffusion effects become dominant and eventually cause the jet to pinch. With the inclusion of diffusion, we observe an interesting phenomena known as the secondary necking. Without surfactant, jet pinches at a location close to the middle of the filament at the left end point of the satellite drop (see Figure 4.1), but the presence of surfactant causes the jet to pinch at a different location (Figure 4.4), also known as a primary and secondary necking. The different pinch-point in the presence of surfactant can have an effect on the dynamics of satellite drops. Figure 4.5 and Figure 4.6 show the surfactant concentration and the surface tension at different times.

4.6 Results with Non-Linear Equation of State

In the previous sections, we used a linear equation of state to express the relationship between the surface tension and the surfactant concentration, which is often appropriate for low or dilute surfactant concentration. In this section, we generalize our earlier analysis to consider a non-linear dependance of the surface tension σ on the surfactant

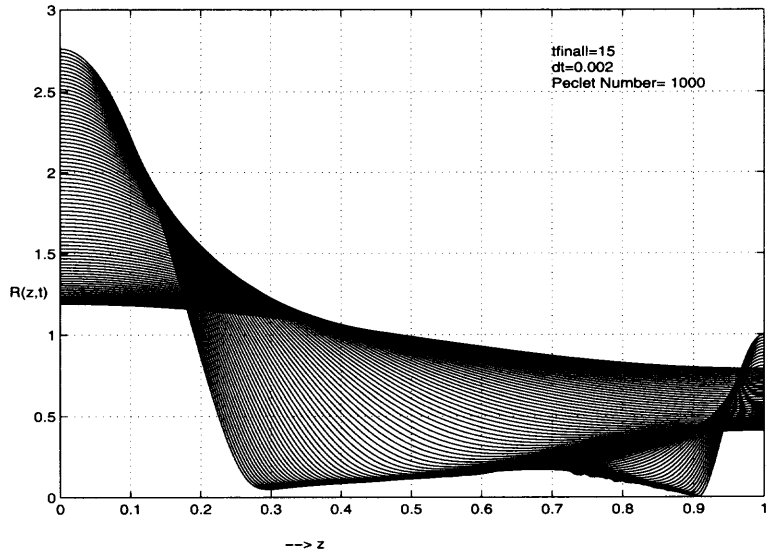

Figure 4.4 Jet radius with diffusion.

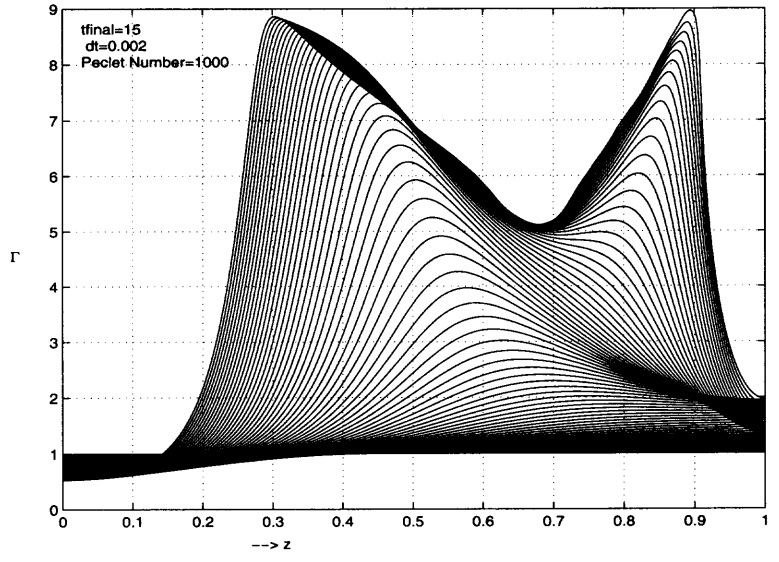

Figure 4.5 Surfactant concentration with diffusion.

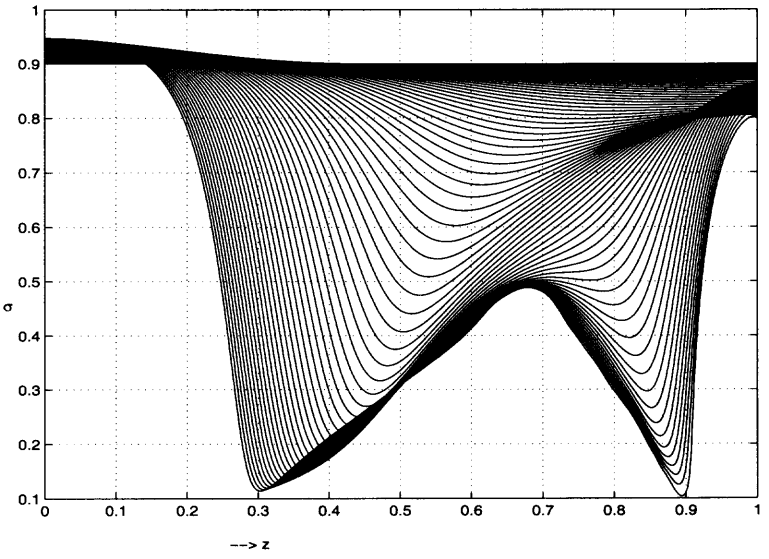

Figure 4.6 Surface tension with diffusion.

concentration Γ. In non-dimensional form it is given by

$$\sigma = 1 + \beta \ln(1 - \Gamma). \tag{4.64}$$

Figure 4.7 shows the result with non-linear equation of state. We see that long wavelength model shows the similar behavior as was observed in the case of linear equation of state, which is indicative of the fact that presence of surfactant retards the pinch-off, irrespective of which equation of state is used.

4.7 Case of Pseudo-Soluble Surfactant

Surfactant solubility, or more specifically, mass transfer of surfactant between the interface and the bulk-phase fluids is not considered in our earlier studies. In this Section, we incorporate the effect of surfactant transfer from the bulk to the interface and vice versa by adding a flux term in the surfactant transport equation.

$$\frac{\partial \Gamma}{\partial t} + \frac{\Gamma}{2R}(Rp_1 - \sigma) = -J, \tag{4.65}$$

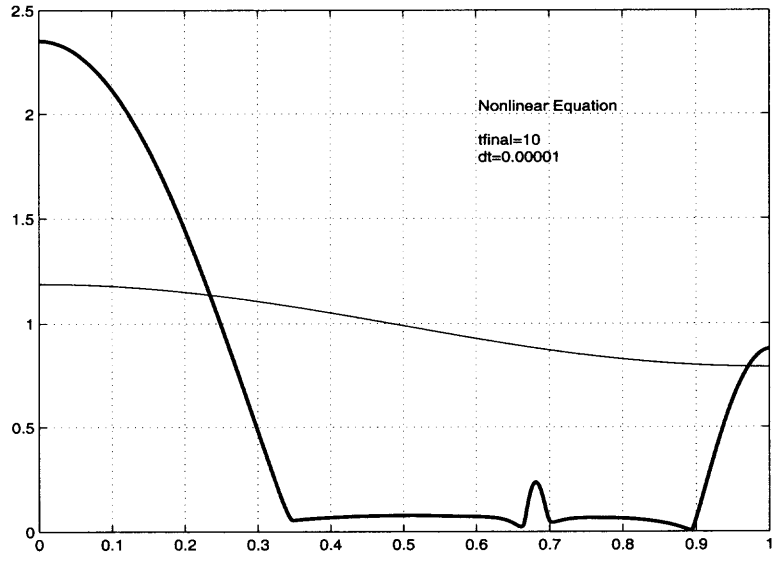

Figure 4.7 Radius of viscous jet with non-linear equation and diffusion.

where the flux onto the interface is given by two steps: first, a diffusive flux bringing surfactant to the interface, $-J_D = D\nabla C.\mathbf{n}$, and second, a kinetic exchange which partitions the surfactant from the sublayer to the interface, $-J_K = \beta C_s(\Gamma_\infty - \Gamma) - \alpha\Gamma$, where D is the diffusion coefficient of surfactant in the bulk, C_s is the sublayer concentration, Γ_∞ is the maximum packing concentration and α, β are desorption and adsorption constants respectively. To write down the equations, we assume that there is a equilibrium between the diffusive flux and the kinetic exchange, i.e., $J_D = J_K$ and either one can be used in the surfactant transport equation.

At equilibrium, $J_K = 0$ gives a relation between the sublayer equilibrium concentration, C_{eq}, and the equilibrium value of surfactant on the interface, Γ_{eq}, i.e.,

$$\beta C_{eq}(\Gamma_\infty - \Gamma_{eq}) = \alpha\Gamma_{eq}. \tag{4.66}$$

Defining the dimensionless equilibrium surfactant concentration $\Gamma_o = \frac{\Gamma_{eq}}{\Gamma_\infty}$, we can rewrite (4.66) as

$$\Gamma_o = \frac{k}{1+k}, \tag{4.67}$$

where we have introduced $k = \frac{\beta C_{eq}}{\alpha}$ and it is a dimensionless measure of the bulk concentration.

To get a governing equation, we add $-J_K$ (or $-J_D$, since they are equal) to the right hand side of (4.65). In this case, we non-dimensionalize Γ by Γ_{eq}, and get the modified surfactant transport equation

$$\frac{\partial \Gamma}{\partial t} + \frac{\Gamma}{2R}(Rp_1 - \sigma) = B_i(1+k)(1-\Gamma), \tag{4.68}$$

where $B_i = \frac{\alpha B \mu}{\sigma_o}$ is a non-dimensional parameter called the Biot number. As an equation of state for σ, we use the following non-dimensional equation of state for the surface tension σ as a function of surface concentration Γ:

$$\sigma = 1 + \tilde{\beta} \ln[1 - \chi\Gamma], \tag{4.69}$$

where $\tilde{\beta} = \frac{RT\Gamma_\infty}{\sigma_o}$ and $\chi = \frac{k}{1+k}$.

We present results in Figures 4.8-4.10 for the jet radius in presence of pseudo-soluble surfactant. We have used $B_i = 1$ and computed the jet radius for different values of χ. Results have consequences in the satellite formation.

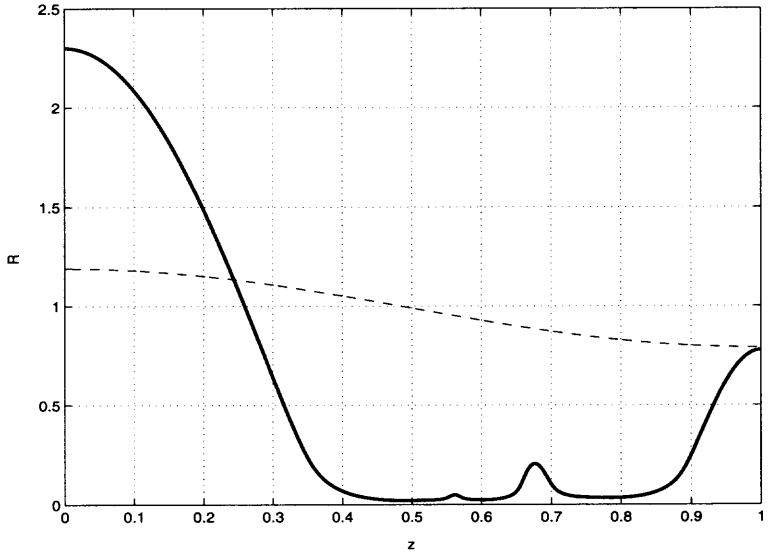

Figure 4.8 Radius of viscous jet with surfactant solubility for $B_i = 1$ and $\chi = 0.9$.

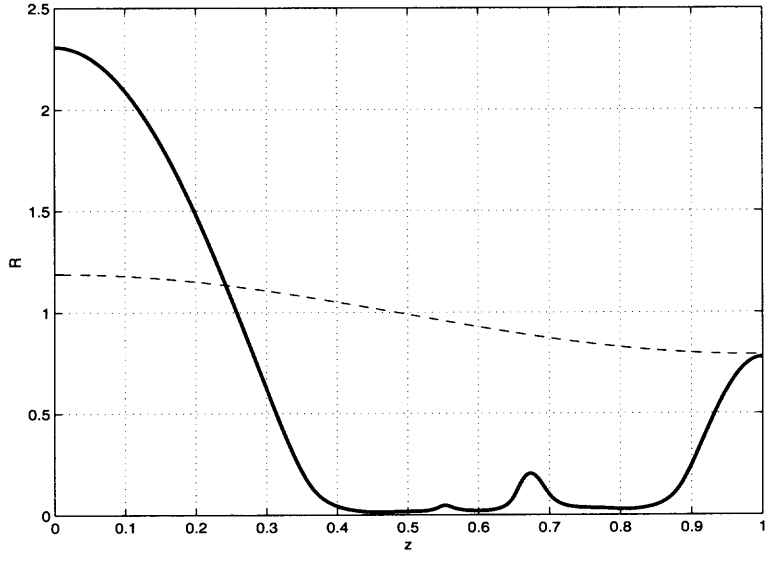

Figure 4.9 Radius of viscous jet with surfactant solubility for $B_i = 1$ and $\chi = 0.99$.

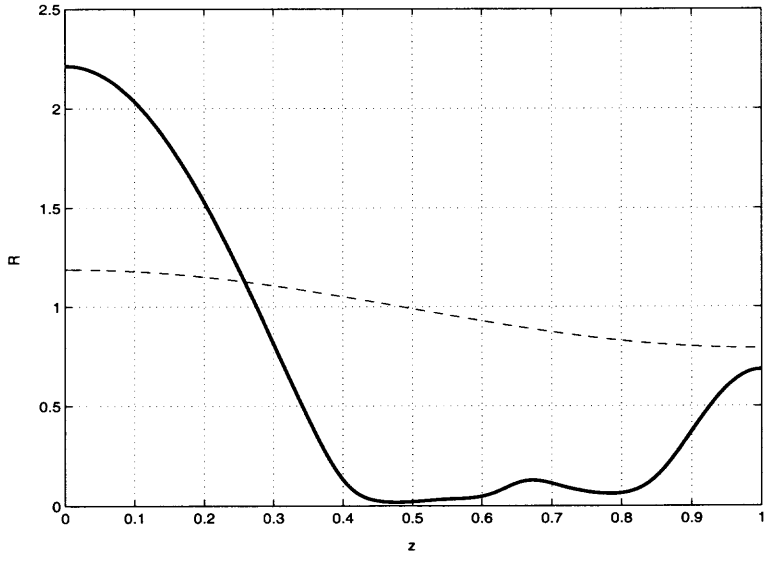

Figure 4.10 Radius of viscous jet with surfactant solubility for $B_i = 1$ and $\chi = 0.999$.

CHAPTER 5

EXPERIMENTAL STUDIES OF JET BREAKUP

This chapter focuses on the experimental studies of the jet breakup. The pendant bubble method is used to measure the evolution and detachment of a bubble for both clean and contaminated interfaces. In this technique, bubbles are formed and grown from the tip of a needle submerged in an exterior fluid. Detachment and necking of the bubble is then observed using a high speed digital camera. A computer analysis of the digitized images is performed to find the minimum neck radius. This system can also be used to determine the surface activity or the interfacial tension between various liquid-liquid or liquid-gas interfaces.

5.1 Experimental Setup

The experimental apparatus mainly consists of a video camera, an image digitizer, a monitor, a PC , a light source and a lens system. In this experiment, air is pumped through a fine stainless steel inverted needle to create a bubble in a viscous liquid. The bubble is formed at the tip needle with a syringe pump which pushes air into a tube connecting the pump to the inverted needle. The capillary tube (needle) is immersed in a glass cell (curvette), which is filled with an aqueous-glycerol mixture. A high speed motion analysis system is used to capture the images of the growing bubble and the break-up process. This motion analysis system is composed of an intensified imager, i.e., camera, and a processor that can record 1000 full frames per second or 12000 partial frames per second. The camera is connected to a video frame grabber that has a resolution of 480×512 pixels. A separate monitor is also connected to the frame grabber in order to view the live images. For the light source, a halogen lamp with constant light intensity is used. A plano-convex lens system is used to produce a collimated beam of light to illuminate the bubble in a glass windowed chamber.

Collimated parallel light passing perpendicularly through the axis of symmetry of the pendant bubble surface, creates the image of the bubble because of the refraction of the light at the bubble surface.

Before starting the actual experiment, the image forming system is calibrated by digitizing a stainless-steel sphere of accurately known diameter. The coordinates of the sphere are measured by the same edge-detection procedure as for the bubble. The horizontal/vertical aspect ratio is a very important parameter in this image analysis method, and is calculated using the images of the sphere. The schematic diagram of the experimental set up is shown in Figure 5.1.

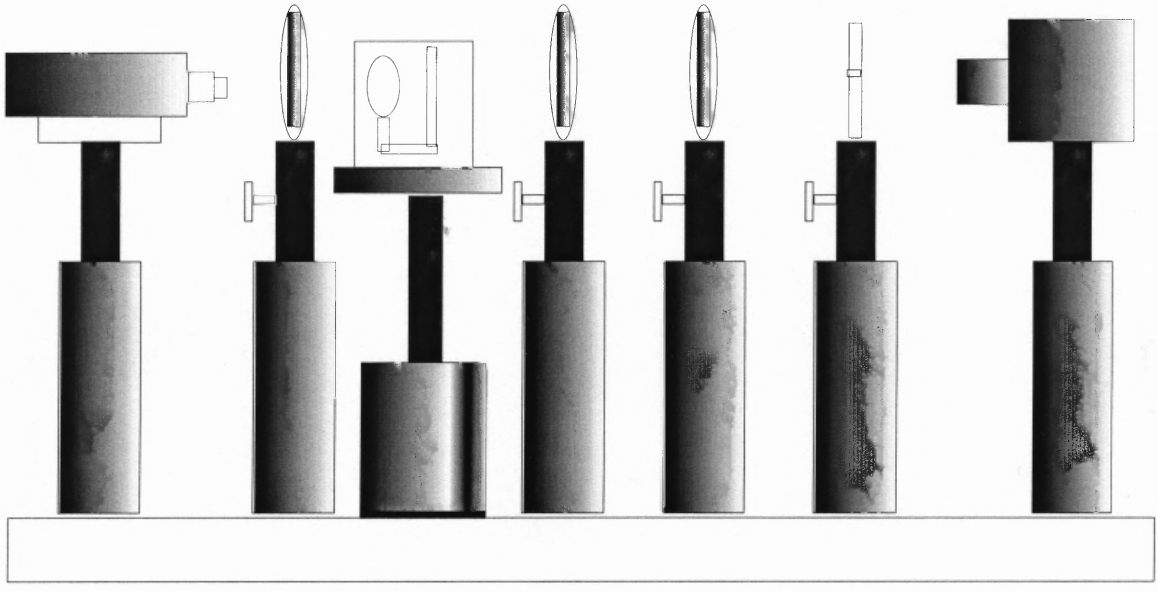

Figure 5.1 Experimental set up.

5.2 Materials and Methods

In preparing the solution for the continuous phase, we choose a glycerine/water mixture with a ratio of 9:1 by volume. We used purified water in our experiments to avoid any kind of impurities. As a surfactant, we use $C_{12}E_0$ in the continuous phase. We used low concentration of surfactant, namely 0.37 mg/lit. All experiments were carried out at a room temperature between $24C^o$ to $27C^o$. The bubbles are formed

using a Cavro digital syringe pump, which is computer controlled. A Hamilton syringe and plunger is placed in the pump in a holder which affixes the barrel to a movable lead screw which moves parallel to the axis of the syringe. By computer control, the lead screw is set in motion, moving the plunger of the syringe down the barrel of the syringe in small programmable increments. The leur lock end of the needle is connected to a two way valve. One end of the valve is connected by Teflon tubing to the inverted needle. The second end is left open and is used to fill the syringe with air.

In the surfactant solution, the bubble is formed and kept there for enough time to allow the surfactant from the surrounding fluid to diffuse onto the bubble interface and to reduce the surface tension. A tiny amount of air is then injected into the bubble to detach it from the needle. The images of the pinching bubble are recorded using a fast video camera.

Measurement of surface tension: The apparatus shown in Figure 5.1 is also called the pendant bubble apparatus and is used to measure the surface tension. To measure the surface tension, a bubble is formed at the tip of an inverted needle with a syringe pump which pushes air into a tube connecting the pump to the needle. The bubble is fully grown to get accurate measurements of the surface tension. The digitized images of the grown bubble are used to detect the locus of the bubble. A digitized image consists of a map of the intensity at each point in the field of the view of the camera which is divided into pixel locations or Cartesian coordinates indicating the row and column positions. The intensity at each pixel location is an integer depending upon A/D converter of the camera; 8 bit converters are normal and the intensity range is from 0-255. A simple program finds the location of the edge by noting when the image intensity drops from brighter liquid value to the darker bubble value. the locus is stored as a set of coordinates. These coordinates are converted to the physical dimensions (in microns) referenced to the origin by calibrating the

field of view. Calibration is undertaken by imaging a spherical ball of known radius. The shape of an axisymmetric pendant bubble depends upon a single parameter, the Bond number. It is a measure of the relative importance of the gravity to the surface tension in determining the shape of the drop. In order to measure the surface tension, the shape and size of the experimentally obtained digitized images are compared to the theoretical profiles obtained by integrating the Young-Laplace equation.

5.3 Experimental Results

Figures 5.2 and Figure 5.3 show the results of our experimental runs, where we can see the effect of the surfactant on the break up of the inviscid jet. Figure 5.2 shows the last few frames of the breakup process for the clean interface. Figure 5.3 shows the breakup of the jet in the presence of the surfactant. Note that the inverted needle orifice is viewable at the bottom of these figures.

The experimental results support the theory that the presence of a surfactant retards the pinch-off. However, several trends are suggestive: In the results without surfactant, the bubble shape near pinch point takes the form of a parabolic profile up until the pinch-off as predicted by the inviscid jet theory of Doshi et al. [8]. The theory of Doshi et al. predicts that eventually the viscous forces in the interior fluid will blunt the profile. This is not very clearly observed in our experiments. We believe that the reason is that the video frames/sec (1000), is too low to capture the blunting, which occurs very close to the pinch-off.

In contrast, when surfactant is present, the blunting of the initially parabolic profile was observed in every trial, even though the same 1000 frames/sec was used. This suggests that the surfactant causes the slender thread (after blunting) to last longer, and it is suggestive of a retardation of the pinch-off process. Our numerical simulations of the model equations show just this type of effect. Qualitatively, we also find evidence that the surfactant retards the pinch-off by measuring time to the

Figure 5.2 Pinching bubble with clean interface.

Figure 5.3 Pinching bubble with surfactant.

pinch-off (by counting the number of frames to the pinch-off, from a fixed profile in the surfactant and no surfactant system with nearly equivalent radius).

Using image analysis software, we extracted a minimum neck radius close to pinch. Figure 5.4 shows the minimum neck radius plotted as a function of time to pinch. This result shows that for a fixed initial neck radius, the jet with surfactant lasts longer and takes more time to pinch.

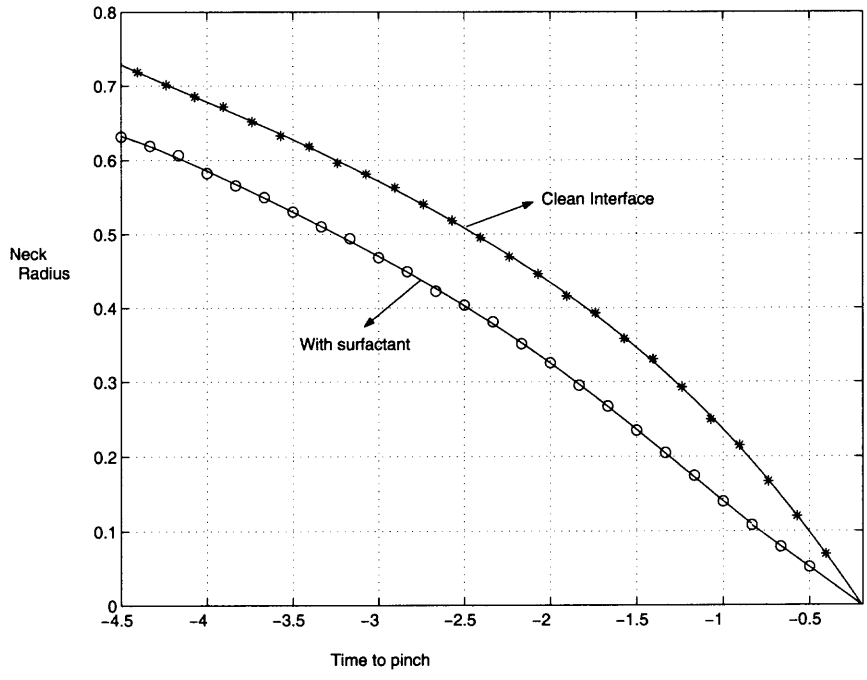

Figure 5.4 Minimum neck radius vs time to pinch.

CHAPTER 6

CONCLUSION AND FUTURE DIRECTIONS

6.1 Conclusions and Discussions

Surface tension driven breakup of a single fluid jet, where the outer medium is assumed to have no effect on the pinching, has been the subject of many investigations [25], [10]. Less work has been focused in understanding the pinch-off of two fluid jets because the presence of the outer fluid makes the problem very complicated and challenging. In this study, we considered the case of a two fluid jet, i.e., the jet which consists of an inner core fluid surrounded by an outer fluid of an infinite extent. The role of a constant as well as variable surface tension, due to the presence of surfactant, is investigated.

We have addressed the effect of an insoluble surfactant on the necking and breakup of a periodic fluid jet. We considered both an inviscid and a slightly viscous jet immersed in a viscous exterior fluid and studied the pinching mechanism and the effect of surfactant on this process. We approached this problem with the tools of the slender body theory and long wavelength asymptotics. It is shown that the slender body theory can be used to construct a mathematical model governing the dynamics of a slender axisymmetric jet.

Instead of considering a full axisymmetric Stokes equations and non-linear boundary conditions, we used non-local slender body theory to reduce Stokes equations, advection diffusion equation for the surfactant transport and non-linear boundary conditions to a simplified one dimensional system of coupled partial differential equations. We analyzed the resulting model both analytically and numerically. This long wave model is then compared with the numerical solution of the full system and it is found that our model captures most of the features of the full problem.

In Chapter 3, we considered a simple case of an inviscid jet and derived a long wavelength model for the evolution of the jet interface and the surfactant concentration. Inside the jet, there is nothing but a passive inviscid fluid with a space independent pressure $p(t)$. Exterior to the slender jet, we have the axisymmetric Stokes equations. Using the slender body theory and asymptotic analysis based upon the slenderness parameter ϵ, we derived a long wave model (Equations 3.43, 3.44). The inside pressure is derived from the condition of the conservation of volume (Equation 3.47).

Numerical Solutions shown in Figure 3.1 and Figure 3.2, represent the jet interface plotted at different time steps. These results show that the presence of surfactant retards the pinch-off and the finite time pinch-off which is observed in the case of a clean interface is inhibited in the formation of a thin and long filament. Figure 3.3 shows the surfactant concentration plotted at various time steps. It shows that in the neck region the surfactant concentration is high as compared to the other regions. Since the total amount of the surfactant is conserved, as the surface area decreases in forming the filament, the amount of surfactant increases by decreasing the surface tension and hence stabilizing the filament. Surprisingly the Marangoni force is not important in the filament formation.

We derived a simple analytical result (3.49), which tells us that with the present long wave model, the pinch-off will not occur. Because if the jet pinches, the surfactant concentration will become unbounded. This indication is confirmed by our numerical simulations, which shows that in presence of the surfactant jet does not pinch.

We also performed a linear stability analysis of the long wavelength model. Linear stability studies agree with the classical result of Tomotika [36] for the case of no surfactant in the long wavelength limit ($k \to 0$). Hansen et al. [14] used a linear stability analysis to study the effect of a soluble surfactant of a two fluid jet. The linear stability results of the long wavelength model can be recovered in the limit $k \to 0$, from Hansen's results, with zero solubility and zero inside viscosity.

The long wave model (Equations 3.43, 3.44) does not predict a pinch-off. If we run the simulations for longer times, the slope of the profiles become steep and eventually develop a shock. Due to large gradients, previously ignored diffusion terms become important and play a significant role in the dynamics. We also included the effect of surface diffusion into the model, characterized by the surface Peclet Number Pe_o. The numerical results show that the presence of surfactant first retards the pinch-off in the formation of a thin and long filament but eventually due to large gradients, the diffusion terms kick in and cause the jet to pinch.

In Chapter 4, we generalized the results of inviscid jet by considering the case of a slightly viscous jet in a highly viscous exterior fluid. The solution exterior to the jet is found by the localized slender body theory, as in the case of inviscid jet. We use lubrication approximations to find the solution inside the jet. The governing equations for the case of a slightly viscous jet (Equations 4.63, 4.64) look similar to that of inviscid jet, but the inside pressure is governed by a boundary value problem for second order ordinary differential equation (Equation 4.65). Numerical results for the case of both with and without surfactant are given in Figure 4.1 and Figure 4.2. These results show the similar behavior of retardation of the pinch-off, as was seen in the case of an inviscid jet. The numerical results show the formation of a thin and long filament, which is stable.

The effect of diffusion is also studied for the case of a slightly viscous jet. Figure 4.4 shows the jet interface in presence of the surfactant with the effect of diffusion. Before the pinch-off, a long neck is formed which eventually pinches due to the surface diffusion triggered by large gradients. It is found that jet with the surfactant and diffusion pinches at a different location as compared to the case of a clean jet. This phenomena is also known as a primary and a secondary necking. Due to the possibility of a high surfactant concentration in the necking region, we also used a non-linear

equation of state (Equation 4.69) to express the relationship between the surface tension and the surfactant concentration.

In Chapter 5, we presented the experimental studies to investigate the breakup of low viscosity jets in a highly viscous exterior fluid. Experimental results support the theory that the presence of the surfactant delays the pinch-off. It is found that for the case of no surfactant, the bubble shape near the pinch point takes the form of parabolic profile up until the pinch-off, as predicted by the theory of Doshi et al. [8]. The theory of Doshi et al. predicts that eventually the viscous forces in the interior fluid will blunt the profile. This is not clearly observed in our experiments. On the other hand, when surfactant is present the blunting of initially parabolic profile is observed in every trial. This suggests that the surfactant causes the slender jet to last longer and thus delays the breakup.

Using the image analysis software, we also extracted minimum neck radius plotted as a function of time to pinch (Figure 5.4). This shows that for a fixed initial neck radius, the jet with the surfactant lasts longer and takes more time to pinch. On average, with the surfactant the pinch-off is delayed approximately by 30% as compared with a clean jet.

6.2 Future Work

6.2.1 Local Similarity Solutions

It will be interesting to extend my work in some other directions. For instance, to perform further analysis of the pinching solutions with surfactant and to find similarity solutions. Experimental observations have revealed that profiles are remarkably similar near the pinch point and are independent of initial conditions. Similarity solutions for the case of constant surface tension have been found by Lister and Sierou [32]. I want to extend my work to find the similarity solution for the case of a variable surface tension, induced by the presence of surfactants.

6.2.2 Surfactant Solubility

All numerical studies described in this work assumed insoluble surfactants. This is a good approximation for soluble surfactants if the bulk concentration is dilute or if the migration to and from the bulk is slow. To gain a better understanding of the jet breakup problem, I want to examine the effect of surfactant solubility, i.e., the surfactant is allowed to transfer between the continuous and the dispersed phases. It is vital to include the effect of surfactant solubility due to two obvious reasons. First, the build-up of surfactant is diminished by transfer of surfactant into the continuous phase. Second, because the adsorption of surfactant occurs at regions of low surfactant concentration and desorption of surfactant occurs from regions of high concentration, this mass transfer of surfactant decreases surfactant gradients [23].

6.2.3 Jet Pinch-off in Presence of Electric Fields and Surfactants

The presence of an electric field is found to have important effects in industrial applications. In chemical and oil industries, the electrostatic fields have been successfully applied to separate the aqueous drops and bubbles from the oil phase [6]. Electrostatic fiber spinning or electrospinning is another important industrial process in which electric fields are used to produce polymeric fibers [31]. Due to increasing technological applications, it is desirable to produce extremely controllable and high quality jets. This is a topic of increasing interest for engineers and physicists in which mechanical, chemical or electrical means are employed to get the desired results. There are some experimental and theoretical studies [21], [20] in which the controlled charged capillary jets of a conducting fluid with different viscosities and applied voltages have been analyzed. The influence of an electric field on the jet breakup especially in presence of surfactant is relatively unexplored. One dimensional long wavelength models have been successfully applied to study the pinching of axisymmetric interfacial jets [25]. These results can be extended to include the effect of electric fields. A model must be provided for effect of electric field on the surfactant evolution.

6.2.4 Deformation of Elastic Membrane

The dynamics of flexible fibers or filaments immersed in a fluid are important in understanding many interesting problems arising in biology, engineering and physics. For instance, in mammals, blood flow in cardiovascular system and air flow in the respiratory system are examples of fluid flows interacting with a flexible and elastic boundary. The interaction between the flow and the flexible surface or membrane is different from that of the rigid surface because of the coupling of the fluid and the membrane dynamics. Previously this problem has been investigated with numerical simulations using immersed boundary method [26]. I want to consider this problem, using asymptotics and long wavelength models to study the deformation of an elastic membrane as a results of its interactions with the flow.

APPENDIX A

MARANGONI TERMS

The Marangoni terms do not appear in the leading order equations. The reason is that the tangential stress balance decouples from the other equations, i.e., f only appears at the leading order in the tangential stress balance. One possible way of incorporating the Marangoni terms into the leading order equations is to rescale various parameters and dependent variables, with a hope that a particular scaling would re-couple the tangential stress balance and Stokeslet density $f(z,t)$ to the other leading order equations.

In this appendix, we show that it is not possible to implement this re-coupling in a consistent asymptotic expansion via a simple rescaling of parameters or variables. Strategy is to find a scaling after the formation of the filament when σ is small. We want to find some scaling (i.e., $\sigma \sim O(\epsilon)$, or $\sigma \sim O(\epsilon^2)$), when f appears at the leading order in some equation other than tangential stress balance. This analysis is done here for the case of $\lambda = 0$.

Suppose R be of $O(1)$ (i.e., we are near the initial evolution). Recall that the surface tension is related to the surfactant concentration by

$$\sigma = 1 - \beta\Gamma \sim \beta\tilde{G}, \tag{A.1}$$

i.e.,

$$\sigma \sim O(\tilde{G}), \tag{A.2}$$

where the order of $\tilde{G}$ is not know at this point.

The leading order tangential stress balance is

$$\frac{4f}{\epsilon R} - \frac{4gR'}{\epsilon R^2} + \frac{4g'}{\epsilon R} = \beta\Gamma_z, \tag{A.3}$$

i.e.,

$$\frac{4f}{\epsilon R} - \frac{4gR'}{\epsilon R^2} + \frac{4g'}{\epsilon R} = \beta \Gamma_z \sim O(\tilde{G}). \tag{A.4}$$

We view A.4 as determining f once Γ and hence σ is known from the surfactant evolution equation (3.50).

The leading order terms in the normal stress balance are

$$p_i - \frac{4g}{\epsilon R^2} + \frac{4\epsilon R' f}{R} = \frac{\sigma}{R}, \tag{A.5}$$

i.e.,

$$p_i - \frac{4g}{\epsilon R^2} + \frac{4\epsilon R' f}{R} \sim O(\tilde{G}). \tag{A.6}$$

Recall the kinematic condition

$$u_r = \epsilon R_t + \epsilon u_z R'. \tag{A.7}$$

Using the values of u_r and u_z from (3.26) and (3.27), the leading order kinematic condition becomes

$$-2\epsilon R f' \ln \frac{1}{\epsilon R} + \frac{2g}{\epsilon R} = \epsilon R_t + 4f\epsilon \ln \frac{1}{\epsilon R}. \tag{A.8}$$

The task now is to pick a scaling for $\tilde{G}$ to get f to appear in some leading order equation other than tangential stress balance with the restriction that $\tilde{G} \lesssim 1$.

Consider first the normal stress balance. Note from (A.4) that either

$$\frac{f}{\epsilon} \sim \frac{g}{\epsilon} \gtrsim \tilde{G} \quad \text{or} \quad f \sim \epsilon \tilde{G}. \tag{A.9}$$

In either case, the third term in (A.6) does not contribute to the leading order in the normal stress balance.

For f to appear in the kinematic condition, we need either

$$\epsilon f \ln \epsilon \gtrsim \frac{g}{\epsilon}, \tag{A.10}$$

or

$$\epsilon f \ln \epsilon \gtrsim \epsilon. \tag{A.11}$$

Using $f \sim \frac{g}{\epsilon^2 \ln \epsilon}$ from (A.10) in the leading order tangential stress balance, we get

$$\frac{g}{\epsilon^2 \ln \epsilon} \sim \tilde{G}. \tag{A.12}$$

Since we have a restriction on $\tilde{G}$ such that $\tilde{G} \lesssim 1$ which along with (A.12) suggests that $g \lesssim \epsilon^2 \ln \epsilon$.

Next, using $f \sim \frac{g}{\epsilon^2 \ln \epsilon}$ in the kinematic condition, we get

$$\frac{g}{\epsilon} \sim \epsilon, \tag{A.13}$$

which suggests that

$$g \sim \epsilon^2. \tag{A.14}$$

Using $f \sim \frac{g}{\epsilon^2 \ln \epsilon}$ from (A.10) and $g \sim \epsilon^2$ from (A.14) in the tangential stress balance, we get

$$\frac{1}{\epsilon \ln \epsilon} \sim \tilde{G}, \tag{A.15}$$

which contradicts with the restriction that $\tilde{G} \leq 1$.

Similarly, if we use $f \sim \frac{1}{\ln \epsilon}$ from (A.11), then from the tangential stress balance we get

$$\frac{1}{\epsilon \ln \epsilon} \sim \tilde{G}, \tag{A.16}$$

but $\tilde{G} \lesssim 1$, which leads to a contradiction.

APPENDIX B

COMPARISON WITH HANSEN

In this appendix, we show that the linear stability analysis of the long wave equations and the linear stability analysis of Hansen et al. [14] are equivalent. The apparent difference is due to the choice of different notations and non-dimensional parameters. We used a linear equation of state, which can be given in dimensional form

$$\sigma = \sigma_o\left(1 - \beta\frac{\Gamma}{\Gamma_o}\right), \tag{B.1}$$

where $\beta = \frac{RT}{\sigma_o}$.

From relation (2.3) of Hansen, we have

$$\sigma = \sigma_o - E_o\left(\frac{\Gamma - \Gamma_o}{\Gamma_o}\right), \tag{B.2}$$

where the σ_o and Γ_o denote the surface tension and the surfactant concentration for the undisturbed thread and E_o is the Gibbs elasticity.

Therefore,

$$\sigma = \sigma_o + E_o - \frac{E_o}{\Gamma_o}\Gamma. \tag{B.3}$$

Rearranging, we get

$$\sigma = \sigma_c\left(1 - \frac{E_o}{\sigma_c\Gamma_o}\Gamma\right), \tag{B.4}$$

where

$$\sigma_c = \sigma_o + E_o. \tag{B.5}$$

Comparing B.1 and B.4, we get

$$\beta = \frac{E_o}{\sigma_c} \quad \Longrightarrow \quad E_o = \beta\sigma_c. \tag{B.6}$$

Hence,

$$\frac{\sigma_o}{E_o} = \frac{\sigma_c - E_o}{E_o}. \tag{B.7}$$

Using B.5, we get

$$\frac{E_o}{\sigma_o} = \frac{\beta}{1-\beta}. \tag{B.8}$$

Recall from Section 3.10, the growth rates obtained from the long wave model are

$$\omega_H = \frac{1-2\beta}{2} \quad \text{and} \quad \omega_H = 0. \tag{B.9}$$

We also derived growth rates from Hansen's analysis, by taking the long wave limit. Growth rates in the Stokes flow limit, represented by ω_S, are found to be

$$\omega_S = \frac{1-2\beta}{2(1-\beta)} \quad \text{and} \quad \omega_H = 0. \tag{B.10}$$

After comparing B.9 and B.10, we find an extra factor of $(1-\beta)$ in ω_S (Hansen's results). Here, we show that this extra factor in the denominator is due to the different non-dimensionalization of time in both studies.

Hansen non-dimensionalised time by

$$T \sim \frac{\rho B^2}{\mu},$$

Therefore, non-dimensional growth rate is

$$\omega_N = \frac{\rho B^2}{\mu}\omega_D, \tag{B.11}$$

where ω_D and ω_N represent the dimensional and the non-dimensional growth rates respectively, and B represents the undisturbed jet radius.

From Hansen, the growth rate for Stokes flow, denoted by ω_S is given by

$$\omega_S = \frac{\omega_N}{N_\sigma}, \tag{B.12}$$

where

$$N_\sigma = \frac{\rho\sigma_o B\mu^2}{\cdot} \tag{B.13}$$

Using B.11 and B.13 in B.12 yields

$$\omega_S = \frac{\mu B}{\sigma_o}\omega_D. \tag{B.14}$$

But from B.5

$$\sigma_o = \sigma_c - E_o.$$

The growth rate for the Stokes flow becomes

$$\omega_S = \frac{\mu B}{\sigma_c(1-\beta)}\omega_D \tag{B.15}$$

In this study, we non-dimensionalize time by $\frac{\mu B}{\sigma_c}$, therefore, the non-dimensional growth rate represented by ω_H, becomes

$$\omega_H = \frac{\mu B}{\sigma_c}\omega_D. \tag{B.16}$$

From B.15 and B.16, we get

$$\omega_H = (1-\beta)\omega_S. \tag{B.17}$$

REFERENCES

[1] ACRIVOS, A., AND LO, T. S. Deformation and breakup of a single slender drop in an extensional flow. *Journal of Fluid Mechanics 86* (1978), 641-672.

[2] BASARAN, O. A. Small-scale free surface flows with breakup: drop formation and emerging applications. *AIChE Journal 48* (2002), 1842-1848.

[3] BLAWZDZIEWICZ, J., CRISTINI, V., AND LOEWENBERG, M. Near-contact motion of surfactant-covered spherical drops: Ionic surfactant. *Journal of Colloid and Interface Science 211* (1996), 355-366.

[4] BUCKMASTER, J. Pointed bubbles in slow viscous flow. *Journal of Fluid Mechanics 55* (1972), 385-400.

[5] COHEN, I., BRENNER, M., E. J., AND NAGEL, S. Two fluid droplet breakup: theory and experiments. *Physical Review Letters 83* (1999), 1147-1150.

[6] COTTRELL, F. G. Process of collecting particles of one liquid suspended in another liquid. *US Patent 987114* (1906).

[7] CRASTER, R. V., MATAR, O. K., AND PAPAGEORGIOU, D. T. Pinchoff and satellite formation in surfactant covered viscous threads. *Physic of Fluids 14* (2002), 1364-1376.

[8] DOSHI, P., COHEN, I., BRENNER, M., SIEGEL, M., HOWELL, P., BASARAN, O., AND NAGEL, R. Persistence of memory in drop breakup: the breakdown of universality. *Science 83* (2003), 1147-1150.

[9] EDWARDS, D. A., BRENNER, H., AND WASAN, D. T. Interfacial transport processes and rheology. *Butterworth-Heinemann* (1991).

[10] EGGERS, J. Universal pinching of 3d axisymmetric free surface flows. *Physical Review Letters 83* (1993), 3458-3460.

[11] EGGERS, J. Nonlinear dynamics and breakup of free surface flows. *Reviews of Modern Physics 69* (1997), 865-929.

[12] FANG, H., AND SHAH, D. O. The effect of surfactant monolayer on the heat transfer through air/water and oil/water interfaces using ir imaging technique. *Journal of Colloid And Interface Science 205* (1998), 531-534.

[13] HANDELSMAN, R., AND KELLER, J. Axially symmetric potential flow around a slender body. *Journal of Fluid Mechanics 28* (1967), 131-147.

[14] HANSEN, S., PETERS, W., AND MEIJER, H. The effect of surfactant on the stability of a fluid filament embedded ina a viscous fluid. *Journal of Fluid Mechanics 382* (1999), 331-349.

[15] HOWELL, P., AND SIEGEL, M. The evolution of a slender non-axisymmetric drop in an extensional flow. *Journal of Fluid Mechanics 521* (2004), 155-180.

[16] KELLER, J., AND RUBINOW, S. Slender body theory for slow viscous flow. *Journal of Fluid Mechanics 75* (1976), 705-714.

[17] KWAK, S., FYRILLAS, M., AND POZRIKIDIS, C. Small-scale free surface flows with breakup: drop formation and emerging applications. *International Journal of Multiphase Flow 27* (2001), 30-60.

[18] KWAK, S., AND POZRIKIDIS, C. Effect of surfactants on the instability of a liquid thread or annular layer. part i. quiescent fluids. *International Journal of Multiphase Flow 27* (2001), 1-37.

[19] LISTER, J., AND STONE, H. Capillary breakup of a viscous thread surrounded by another viscous fluid. *Physics of Fluids 10* (1998), 289-306.

[20] LOPEZ-HERRERA, J. M., AND GANAN-CALVO. A note on a charged capillary jet breakup of conducting liquid: experimental validation of a viscous one dimensional model. *Journal of Fluid Mechanics 83* (2004), 303-326.

[21] LOPEZ-HERRERA, J. M., GANAN-CALVO, A. M., AND PEREZ-SABORID, M. One dimensional simulation of the breakup of capillary jets of conducting liquids: application to e.h.d spraying. *Journal of Aerosol Science 30* (1999), 895-912.

[22] MILLIKEN, W., STONE, H., AND LEAL, L. The effect of surfactant on the transient motion of newtonian drops. *Physics of Fluids 5* (1993), 69-79.

[23] MILLIKEN, W. J., AND LEAL, L. G. The influence of surfactant on the deformation and breakup of a viscous drop: the effect of surfactant solubility. *Journal of Colloid and Interface Science 166* (1994), 275-285.

[24] PAN, R., GREEN, J., AND MALDARELLI, C. Theory and experiment on the measurement of kinetic rate constants for surfactant exchange at an air/water interface. *Journal of Colloid And Interface Science 205* (1998), 213-230.

[25] PAPAGEORGIOU, D. On the breakup of viscous liquid threads. *Physics of Fluids 7* (1995), 1529-1544.

[26] PESKIN, C. S. Numerical analysis of blood flow in the heart. *Journal of Computational Physics 25* (1977), 220-255.

[27] POZRIKIDIS, C. Boundary integral and singularity methods for linearized viscous flow. *Cambridge University Press* (1992).

[28] RAYLEIGH, L. On the stability of jets. *Proc. Lond. Math. Soc. 10* (1878), 4-13.

[29] ROTHERT, A., RICHTER, R., AND REHBERG, I. Formation of a drop: viscosity dependence of three flow regimes. *New Journal of Physics 5* (2003), 1-59.

[30] RUST, A. C., AND MANGA, M. Bubble shapes and orientations in low Re simple shear flow. *Journal of Colloid and Interface Science 249* (2002), 476-480.

[31] SHIN, M. Y., HOHMAN, M. M., BRENNER, M., AND RUTLEDGE, G. C. Electrospinning: a whipping fluid jet generates submicron polymer fibers. *Applied Physics Letters 78* (2001), 1-3.

[32] SIEROU, A., AND LISTER, J. Self-similar solutions for viscous capillary pinch-off. *Journal of Fluid Mechanics 497* (2003), 381-403.

[33] STONE, H. A simple derivation of the time dependent convection-diffusion equation for surfactant transport along a deforming interface. *Physics of Fluids 2* (1990), 111-112.

[34] STONE, H., AND LEAL, G. The effect of surfactants on drop deformation and breakup. *Journal of Fluid Mechanics 222* (1990), 65-102.

[35] TIMMERMANS, M., AND LISTER, J. The effect of surfactant on stability of a liquid thread. *Journal of Fluid Mechanics 459* (2002), 289-306.

[36] TOMOTIKA, S. On the stability of a cylindrical thread of a viscous fluid surrounded by another viscous fluid. *Proceedings of Royal Society of London A 150* (1935), 322-337.

[37] WEBER, C. On the breakdown of liquid jet. *Z. Angew. Math. Phys.* (1931), 11-14.

[38] WEBSTER, D. R., AND LONGMIRE, E. K. Jet pinch-off and drop formation in immiscible liquid-liquid systems. *Experiments in Fluids 30* (2001), 47-56.

[39] WHITAKER, S. Studies of the drop-weight method for surfactant solutions. *Journal of colloid and interfacial science 51* (1976), 231-248.

[40] WONG, H., RUMSCHITZKI, D., AND MALDARELLI, C. On the surfactant mass balance at a deforming fluid interface. *Physics of Fluids 8* (1996), 3203-3204.

[41] ZHANG, W. Singularities in free surface flows. *Harvard University, Ph.D Thesis* (2000).

[42] ZHANG, W., AND LISTER, J. Similarity solutions for capillary pinchoff in fluids of differing viscosity. *Physics Review Letters 83* (1999), 1151-1154.